

---

# SiGeo: SUB-ONE-SHOT NAS VIA INFORMATION THEORY AND GEOMETRY OF LOSS LANDSCAPE

---

A PREPRINT

Hua Zheng<sup>1\*</sup>, Kuang-Hung Liu<sup>2</sup>, Igor Fedorov<sup>2</sup>, Xin Zhang<sup>2</sup>, Wen-Yen Chen<sup>2</sup>, Wei Wen<sup>2</sup>  
Northeastern University<sup>1</sup>, Meta AI<sup>2</sup>  
zheng.hua1@northeastern.edu, {khliu, ifedorov, wewen, wychen}@meta.com

November 23, 2023

## ABSTRACT

Neural Architecture Search (NAS) has become a widely used tool for automating neural network design. While one-shot NAS methods have successfully reduced computational requirements, they often require extensive training. On the other hand, zero-shot NAS utilizes training-free proxies to evaluate a candidate architecture’s test performance but has two limitations: (1) inability to use the information gained as a network improves with training and (2) unreliable performance, particularly in complex domains like RecSys, due to the multi-modal data inputs and complex architecture configurations. To synthesize the benefits of both methods, we introduce a “sub-one-shot” paradigm that serves as a bridge between zero-shot and one-shot NAS. In sub-one-shot NAS, the supernet is trained using only a small subset of the training data, a phase we refer to as “warm-up.” Within this framework, we present SiGeo, a proxy founded on a novel theoretical framework that connects the supernet warm-up with the efficacy of the proxy. Extensive experiments have shown that SiGeo, with the benefit of warm-up, consistently outperforms state-of-the-art NAS proxies on various established NAS benchmarks. When a supernet is warmed up, it can achieve comparable performance to weight-sharing one-shot NAS methods, but with a significant reduction ( $\sim 60\%$ ) in computational costs.

## 1 Introduction

In recent years, Neural Architecture Search (NAS) has emerged as a pivotal paradigm for automating the design of neural networks. One-shot NAS simplifies the process of designing neural networks by using a single, comprehensive supernet (i.e. search space), which contains a versatile choice of candidate architectures. This approach allows for quick evaluation of various network architectures, saving both time and computational resources. It has been successfully applied to the vision domain [Liu et al., 2018, Real et al., 2017, Cai et al., 2020, Chitty-Venkata et al., 2022, Fedorov et al., 2022] and RecSys domain [Krishna et al., 2021, Zhang et al., 2023, Song et al., 2020]. One-shot NAS speeds up the process of finding the best neural network design, but it still requires training [Li et al., 2023]. To mitigate this, zero-shot Neural Architecture Search (zero-shot NAS) has been developed with the aim of bypassing the need for extensive training and evaluation. The core of zero-shot NAS is to use a zero-cost metric to quickly evaluate the actual performance of candidate architectures. While a wide range of zero-shot proxies have been introduced, a recent study [White et al., 2022] has suggested that many of them do not fully utilize the information gained as a network improves with training. As a result, the pretraining of a supernet does not necessarily translate into enhanced search performance, leaving an unexplored opportunity for improvement.

Despite significant advances in zero-shot NAS in the computer vision domain, its application to other complex domains, such as recommendation systems (RecSys), remains largely underexplored. RecSys models introduce unique challenges, primarily owing to their multi-modal data inputs and the diversity in their architectural configurations Zhang et al. [2023]. Unlike vision models, which generally rely on homogeneous 3D tensors, RecSys handles multi-modal features, a blend of 2D and 3D tensors. Additionally, vision models predominantly utilize convolutional layers,

---

\*This work was done when the first author was an intern at Meta

whereas RecSys models are heterogeneous within each stage of the model using a variety of building blocks, including but not limited to Sum, Gating, Dot-Product, and Multi-Head Attention. This added complexity makes the naive deployment of state-of-the-art (SOTA) zero-shot NAS approaches less effective in the recommendation context.

Table 1: Comparison of SiGeo v.s. existing NAS methods for RecSys

Method	Setting	Criteo Log Loss	Avazu Log Loss	KDD Log Loss	GPU Days
PROFIT [Gao et al., 2021]	One-shot	0.4427	0.3735	-	~0.5
AutoCTR [Song et al., 2020]	One-shot	0.4413	0.3800	0.1520	~0.75
NASRecNet [Zhang et al., 2023]	One-shot	0.4395	0.3736	0.1487	~0.3
ZiCo [Li et al., 2023]	Zero-shot	0.4404	0.3770	0.1486	~0.11
SiGeo (Ours)	Zero-Shot	0.4404	0.3750	0.1486	~0.11
	Sub-one-shot	0.4396	0.3741	0.1484	~0.12

To mitigate the limitations of existing NAS methods, this work presents a novel sub-one-shot search strategy. As a setting between zero-shot and one-shot, sub-one-shot NAS allows for limited training of supernet with a small portion of data while still employing a training-free proxy for performance prediction of sampled subnets, as illustrated in Fig. 1. Therefore, the sub-one-shot NAS considers a trade-off between computational efficiency and predictive performance. In order to effectively utilize the additional information inherited from the pretrained supernet, we further develop a new Sub-one-shot proxy based on the information theory and **Geometry** of loss landscape, named **SiGeo**. In sum, this work makes the following contributions:

- We introduce SiGeo, a novel proxy proven to be effective in NAS when the candidate architectures are warmed up.
- We theoretically analyze the geometry of loss landscapes and demonstrate the connection between the warm-up of supernet and the effectiveness of the SiGeo.
- Sub-one-shot setting is proposed to bridge the gap between zero-shot and one-shot NAS.
- Extensive experiments are conducted to assess the effectiveness of SiGeo in both CV and RecSys domains under the sub-one-shot setting. The results show that as we increase the warm-up level, SiGeo’s scores align more closely with test accuracies. Compared with the weight-sharing one-shot NAS, SiGeo shows comparable performance but with a significant reduction in computational costs, as shown in Table 1.

## 2 Problem Description and Related Work

**One-Shot NAS** One-shot NAS algorithms [Brock et al., 2018] train a weight sharing supernet, which jointly optimizes subnets in neural architecture search space. Then this supernet is used to guide the selection of candidate architectures. Let  $\mathcal{A}$  denote the architecture search space and  $\Theta$  as all learnable weights. Let  $\ell$  denote the loss function. The goal of one-shot training is to solve the following optimization problem under the given resource constraint  $r$ :

$$\Theta^* = \arg \min_{\Theta} \mathbb{E}_{\mathbf{a} \sim \mathcal{A}} [\ell(\mathbf{a} | \Theta_{\mathbf{a}}, \mathcal{D})]$$

$$\mathbf{a}^* = \arg \max_{\mathbf{a} \in \mathcal{A}} \mathcal{P}_{score}(\mathbf{a} | \Theta_{\mathbf{a}}^*; \mathcal{D}_{val}) \quad \text{s.t.} \quad R(\mathbf{a}) \leq r$$

where  $\mathbf{a}$  is the candidate architecture (i.e. subnet) sampled from the search space  $\mathcal{A}$ ,  $\Theta_{\mathbf{a}} \in \Theta$  is the corresponding part of inherited weights (i.e. subnet) and  $R(\cdot)$  represents the resource consumption, i.e. latency and FLOPs.  $\mathcal{P}_{score}$  evaluates performance on the validation dataset. There are many methods proposed for CV tasks [Chen et al., 2019, Dong and Yang, 2019, Cai et al., 2019, Stamoulis et al., 2019, Li et al., 2020, Chu et al., 2021, Guo et al., 2020, Fedorov et al., 2022, Banbury et al., 2021], natural language processing [So et al., 2019, Wang et al., 2020a], and RecSys task [Gao et al., 2021, Krishna et al., 2021, Zhang et al., 2023, Song et al., 2020].

**Zero-Shot NAS** Zero-shot NAS proxies have been introduced, aiming to predict the quality of candidate architectures without the need for any training. Zero-shot NAS can be formulated as

$$\mathbf{a}^* = \arg \max_{\mathbf{a} \in \mathcal{A}} \mathcal{P}_{zero}(\mathbf{a} | \Theta_{\mathbf{a}}) \quad \text{s.t.} \quad R(\mathbf{a}) \leq r$$

where  $\mathcal{P}_{zero}$  is a zero-shot proxy function that can quickly measure the performance of any given candidate architecture without training. Some existing proxies measure the expressivity of a deep neural network [Mellor et al., 2021,

Chen et al., 2021, Bhardwaj et al., 2022, Lin et al., 2021a] while many proxies rely on gradient of network parameter [Abdelfattah et al., 2021, Lee et al., 2019, Tanaka et al., 2020, Wang et al., 2020b, Lopes et al., 2021]. Recently, Li et al. [2023] introduced ZiCo, a zero-shot proxy based on the relative standard deviation of the gradient. This approach has been shown to be consistently better than other zero-shot proxies.

**Sub-One-Shot NAS** For the weight-sharing NAS, one key difference between one-shot and zero-shot settings is the warm-up phase. In a one-shot NAS, the supernet is trained using a large dataset. However, as noted by [Wang et al., 2023], “training within a huge sample space damages the performance of individual subnets and requires more computation to search”. Conversely, the zero-shot setting omits this warm-up phase, leading to a more efficient process. Nonetheless, the performance of zero-shot proxies is often less reliable and subject to task-specific limitations. To bridge the gap, we propose a new setting called “sub-one-shot”, where the supernet is allowed to be warmed up by a small portion of training data (e.g. 1% training samples) prior to the search process. Our goal is to propose a new proxy that can work in both zero-shot and sub-one-shot settings; see Fig. 1a.

**Other Hybrid NAS** Recently, Wang et al. [2023] proposed PreNAS to reduce the search space by a zero-cost selector before performing the weight-sharing one-shot training on the selected architectures to alleviate gradient update conflicts [Gong et al., 2021].

**Remark 1.** Compared with other zero-shot proxies, SiGeo allows for the supernet warm-up. In practice, the warm-up with 1-10% data is enough to make SiGeo achieve the SOTA performance.

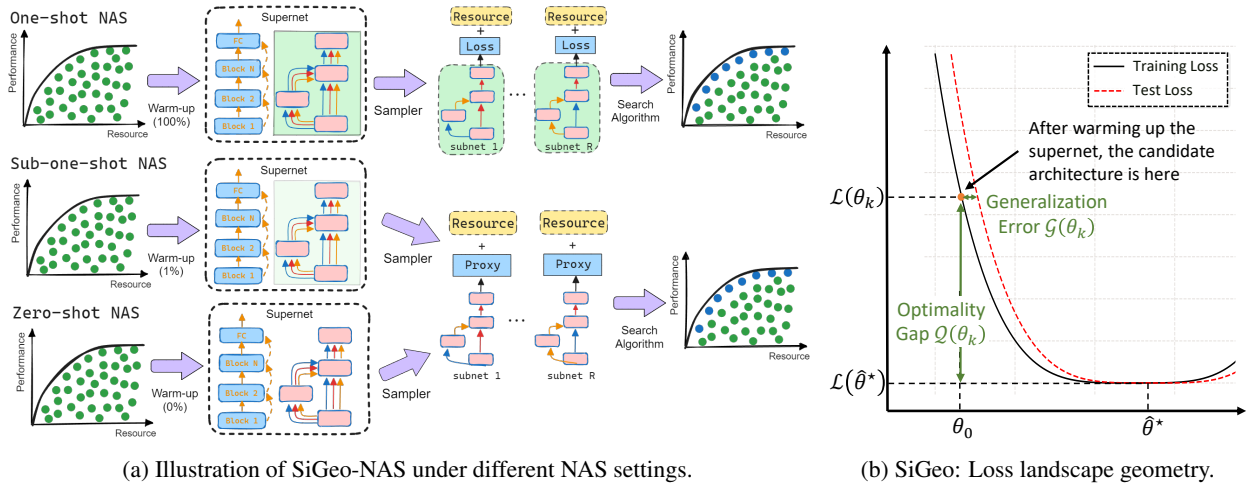


Figure 1: (a) SiGeo-NAS samples candidate architectures in the search space with a light warm-up. In comparison to the resource-intensive one-shot training of the supernet, this strategy offers an efficient and cost-effective means of evaluating subnets within evolution search or reinforcement learning (RL) search. In contrast to the conventional zero-shot approach, SiGeo-NAS attains notably improved performance while incurring only a minimal warm-up cost. (b) The connection between SiGeo and the geometry of loss landscape around the local minimum. The test error is approximated by the minimum achievable training loss and the generalization error.

**Information Matrix and Fisher-Rao Norm** Define  $q : \mathcal{X} \times \mathcal{Y} \rightarrow \mathbb{R}$  as the probability function of *true* data distribution. The probability function of the model distribution is defined as  $p_\theta(\mathbf{x}, \mathbf{y}) = q(\mathbf{x})p_\theta(\mathbf{y}|\mathbf{x})$ , with the marginal input distribution  $q(\mathbf{x})$  and the conditional distribution  $p_\theta(\mathbf{y}|\mathbf{x})$ . Fisher information matrix  $\mathbf{F}$  and the Hessian  $\mathbf{H}$  are defined as [Thomas et al., 2020],

$$\mathbf{F}(\theta) = \mathbb{E}_{p_\theta} \left[ \frac{\partial^2 \ell(\theta; \mathbf{x}, \mathbf{y})}{\partial \theta \partial \theta^\top} \right] = \mathbb{E}_{p_\theta} \left[ \frac{\partial}{\partial \theta} \ell(\theta; \mathbf{x}, \mathbf{y}) \frac{\partial}{\partial \theta} \ell(\theta; \mathbf{x}, \mathbf{y})^\top \right] \text{ and } \mathbf{H}(\theta) = \mathbb{E}_q \left[ \frac{\partial^2 \ell(\theta; \mathbf{x}, \mathbf{y})}{\partial \theta \partial \theta^\top} \right] \quad (1)$$

It has been shown that Fisher and Hessian matrices are identical when the learned model distribution becomes the same as the true sampling distribution [Lee et al., 2022, Karakida et al., 2019, Thomas et al., 2020]. Thomas et al. [2020] has shown that these two matrices are empirically close as training progresses. The Fisher-Rao (FR) norm, defined as  $\|\theta\|_{fr} := \theta^\top \mathbf{F}(\theta) \theta$ , has been proposed as a measure of the generalization capacity of deep neural networks (DNNs) Liang et al. [2019].

**Notation.** Here we briefly summarize the notations in the paper. For any matrix  $\mathbf{A}$ , we use  $\|\mathbf{A}\|$ , and  $\|\mathbf{A}\|_F$  to denote its operator norm and Frobenius norm, respectively. In addition, the eigenvalues  $\lambda_i(\mathbf{A})$  of matrix  $\mathbf{A}$  are sorted in non-ascending order, i.e.  $\lambda_1 \geq \lambda_2 \geq \dots \geq \lambda_d$ . Unless otherwise specified, we use  $\mathbb{E}[\cdot]$  to denote the expectation over

the joint distribution of all samples accumulated in the training process to date, often referred to as the filtration in stochastic approximation literature. In what follows, we use  $\oslash$  to denote the element-wise division and  $\nabla$  to represent  $\nabla_{\theta}$ .

### 3 Convergence and Generalization

After the warm-up phase (i.e. the supernet is trained using a small subset of the training data), the weight of the supernet will escape the saddle points and reside near a certain local minimum denoted by  $\hat{\theta}^*$  [Fang et al., 2019, Kleinberg et al., 2018, Xu et al., 2018]. This observation motivates us to focus on the convergence phase of learning algorithms, leading directly to the assumption **A.2**.

For each candidate architecture  $\alpha$  associated with the weight  $\theta := \Theta_{\alpha} \in \Theta$ , consider a supervised learning problem of predicting outputs  $\mathbf{y} \in \mathcal{Y}$  from inputs  $\mathbf{x} \in \mathcal{X}$ . Let  $\hat{\theta}^*$  denote the local minimum near which the weight of subnet is located. Given  $N$  i.i.d training samples  $\mathcal{D} = \{(\mathbf{x}_n, \mathbf{y}_n); n = 1, \dots, N\}$ , the training objective is to minimize the empirical training loss starting with an initial weight  $\theta_0$  inherited from the pretrained supernet as follows

$$\hat{\theta}^* \in \arg \min_{\theta \in \mathbb{R}^d} \ell(\theta; \mathcal{D}) := \mathbb{E}_{\hat{q}}[\ell(\theta; \mathbf{x}, \mathbf{y})] = \frac{1}{N} \sum_{n=1}^N \ell(\theta; \mathbf{x}_n, \mathbf{y}_n) \quad (2)$$

where  $\hat{q}$  is the empirical distribution and  $\ell(\theta; \mathbf{x}, \mathbf{y})$  is the loss function. Define the expected loss as  $\mathcal{L}(\theta) = \mathbb{E}_q[\ell(\theta; \mathbf{x}, \mathbf{y})]$ , which can be decomposed at a true local minimum  $\theta^* = \arg \min_{\theta \in \mathbb{R}^d} \mathcal{L}(\theta)$ :

$$\mathcal{L}(\theta^*) = \underbrace{\mathbb{E}_q[\ell(\theta^*; \mathbf{x}, \mathbf{y}) - \ell(\hat{\theta}^*; \mathbf{x}, \mathbf{y})]}_{\text{Excess Risk}} + \underbrace{\mathbb{E}_q[\ell(\hat{\theta}^*; \mathbf{x}, \mathbf{y})] - \mathbb{E}_{\hat{q}}[\ell(\hat{\theta}^*; \mathbf{x}, \mathbf{y})]}_{\text{Generalization Error}} + \underbrace{\mathbb{E}_{\hat{q}}[\ell(\hat{\theta}^*; \mathbf{x}, \mathbf{y})]}_{\text{Training Loss}} \quad (3)$$

where the first term represents the *excess risk*, the difference between test error and the minimum possible error. The second term is *generalization error* measuring the difference between train and test error and indicating the extent to which the classifier may be overfitted to a specific training set. The last term is the *training loss*. We aim to derive a proxy that measures  $\mathcal{L}(\theta^*)$  using training-free estimators of the training loss and generalization error.

To facilitate the analysis, we introduce assumptions (**A.2-A.4**) that the initial weight inherited from the supernet remains within a compact space, where the training loss is differentiable and has positive definite Hessian around  $\hat{\theta}^*$ . We study the asymptotic behavior of iterations of the form

$$\theta_{k+1} \leftarrow \theta_k - \eta_k \mathbf{B}_k^{-1} \nabla \ell(\theta_k; \mathcal{D}_k) \quad (4)$$

where  $\mathbf{B}_k$  is a curvature matrix and  $\nabla \ell(\theta_k; \mathcal{D}_k) = \frac{1}{|\mathcal{D}_k|} \sum_{(\mathbf{x}_n, \mathbf{y}_n) \in \mathcal{D}_k} \nabla \ell(\theta_k; \mathbf{x}_n, \mathbf{y}_n)$  is a sample gradient estimate from a uniformly sampled mini-batch  $\mathcal{D}_k \subseteq \mathcal{D}$  at iteration  $k$ . Eq. 4 becomes a first-order stochastic gradient descent (SGD) if the curvature function is an identity matrix,  $\mathbf{B}_k = \mathbf{I}$ . It turns out to be a natural gradient descent if the curvature function is the exact Fisher information matrix  $\mathbf{B}_k = \mathbf{F}$  and second-order optimization if  $\mathbf{B}_k$  is the Hessian [Martens, 2020].

#### 3.1 Regularity Conditions

We summarize the assumptions for the regularity of stochastic gradient descent, serving as the foundation for our analysis. The justification for the assumption can be found in Appendix A.

- A.1** (Realizability) The true data-generating distribution is in the model class.
- A.2** (Initiation) The initial weight of the candidate architecture,  $\theta_0$ , (probably after the warm-up) is located within a compact set  $\mathbb{B}$  centered at  $\hat{\theta}^*$ , such that  $\|\theta_0 - \hat{\theta}^*\|_1 \leq M$ .
- A.3** (Differentiability) The loss function of candidate network  $\ell(\theta; \mathbf{x}, \mathbf{y})$  is differentiable almost everywhere on  $\theta \in \mathbb{B}$  for all  $(\mathbf{x}, \mathbf{y}) \in \mathcal{X} \times \mathcal{Y}$ .
- A.4** (Invertibility) The Hessian, Fisher's information matrix and covariance matrix of the gradient are positive definite in the parametric space  $\mathbb{B}$  such that they are invertible.

#### 3.2 On Convergence of Training Loss

Now let's analyze the convergence rate for a given candidate architecture and investigate the impact of gradient variance. Let  $\mathcal{Q}(\theta) := \mathcal{L}(\theta) - \mathcal{L}(\hat{\theta}^*) = \mathbb{E}[\ell(\theta; \mathbf{x}, \mathbf{y})] - \mathbb{E}[\ell(\hat{\theta}^*; \mathbf{x}, \mathbf{y})]$  denote the (local) optimality gap from the local

minimum loss. The following theorem presents the rate of convergence by using a similar technique as Garrigos and Gower [2023, Theorem 5.3.].

**Theorem 1.** *Assume A.1-A.4. Consider  $\{\theta_k\}_{k \in \mathbb{Z}}$  a sequence generated by the first-order (SGD) algorithm (4), with a decreasing sequence of stepsizes satisfying  $\eta_k > 0$ . Let  $\sigma_k^2 := \text{Var}[\nabla \ell(\theta_k; \mathcal{D}_k)]$  denote the variance of sample gradient, where the variance is taken over the joint distribution of all the training samples until the  $k$ -th iteration. Then It holds that*

$$\mathbb{E}[\mathcal{L}(\bar{\theta}_k)] - \mathcal{L}(\hat{\theta}^*) \leq \frac{\|\theta_0 - \hat{\theta}^*\|}{2 \sum_{i=0}^{k-1} \eta_i} + \frac{1}{2} \sum_{i=0}^{k-1} \sigma_i^2$$

The proof of Theorem 1 is provided in Appendix B. The key insight from this theorem is the relationship between the optimality gap and the gradient variance. In particular, the smaller the gradient variance across different training samples, the lower the training loss the model converges to; i.e., the network converges at a faster rate. In Section 3.4, we'll further discuss how the gradient variance is related to the Hessian matrix around local minima, thereby representing the curvature of the local minimum as shown in [Thomas et al., 2020].

Owing to the page limit, a comprehensive study on the convergence rate under the strong convexity assumption can be found in Appendix C. Beyond the gradient variance, this study provides insight into the relationship between the rate of convergence and the FR norm. Specifically, Theorem4 in Appendix C illustrates that a higher FR norm across training samples leads to a lower convergence point in training loss, signifying a quicker convergence rate.

### 3.3 Lower Bound of Minimum Achievable Training Loss

This section examines the loss landscape to provide insights into predicting the minimum achievable training loss for a candidate architecture. The discussion follows the similar analysis technique used by Martens [2020]. Applying Taylor's approximation to the expected loss function  $\mathcal{L}(\theta)$  gives

$$\begin{aligned} \mathcal{L}(\theta_k) - \mathcal{L}(\hat{\theta}^*) &= \frac{1}{2} (\theta_k - \hat{\theta}^*)^\top \mathbf{H}(\hat{\theta}^*) (\theta_k - \hat{\theta}^*) + \nabla \mathcal{L}(\hat{\theta}^*)^\top (\theta_k - \hat{\theta}^*) + \mathcal{O} \left( (\theta_k - \hat{\theta}^*)^3 \right) \\ &= \frac{1}{2} (\theta_k - \hat{\theta}^*)^\top \mathbf{H}(\hat{\theta}^*) (\theta_k - \hat{\theta}^*) + \mathcal{O} \left( (\theta_k - \hat{\theta}^*)^3 \right) \end{aligned} \quad (5)$$

where the last inequality holds due to  $\nabla \mathcal{L}(\hat{\theta}^*) = 0$ . By taking the expectation over the joint distribution of all samples used for training until  $k$ -th iteration, the optimality gap (Eq. 5) becomes

$$\mathcal{Q}_k := \mathbb{E}[\mathcal{L}(\theta_k)] - \mathcal{L}(\hat{\theta}^*) = \frac{1}{2} \mathbb{E} \left[ (\theta_k - \hat{\theta}^*)^\top \mathbf{H}(\hat{\theta}^*) (\theta_k - \hat{\theta}^*) \right] + \mathbb{E} \left[ \mathcal{O} \left( (\theta_k - \hat{\theta}^*)^3 \right) \right]. \quad (6)$$

By assuming the local convexity (A.4) and some mild conditions, it holds  $\mathbb{E} \left[ \|\theta_k - \hat{\theta}^*\|^2 \right] = \mathcal{O}(\frac{1}{k})$ ; see details in Lacoste-Julien et al. [2012, Theorem 4] or Bottou and Le Cun [2005, Theorem A3]. It implies that the higher order term  $\mathbb{E} \left[ (\theta_k - \hat{\theta}^*)^3 \right]$  would shrink faster, that is,  $\mathbb{E} \left[ (\theta_k - \hat{\theta}^*)^3 \right] = o(\frac{1}{k})$  [Martens, 2020]. As a result, it is sufficient to focus on a quadratic loss and then present the lower bound of the minimum achievable training loss; see the proof of Theorem 2 in Appendix D.

**Theorem 2.** *Assume A.1-A.4. Let  $\mu_k = \sum_{i=0}^k \mathbb{E} [\|\nabla \ell(\theta_i; \mathcal{D}_i)\|_1]$  denote the sum of the expected absolute value of gradient across mini-batch samples, denoted by  $\mathcal{D}_i$ , where the gradient norm is*

$$\|\nabla \ell(\theta_i; \mathcal{D}_i)\|_1 = \sum_{j=1}^d \left| \nabla_{\theta_i^{(j)}} \ell(\theta_i; \mathcal{D}_i) \right| \quad \text{and} \quad \nabla_{\theta_i^{(j)}} \ell(\theta_i; \mathcal{D}_i) = \frac{1}{|\mathcal{D}_i|} \sum_{n=1}^{|\mathcal{D}_i|} \nabla_{\theta_i^{(j)}} \ell(\theta_i; \mathbf{x}_n, \mathbf{y}_n).$$

Under some regularity conditions such that  $\mathbb{E} \left[ (\theta_k - \hat{\theta}^*)^3 \right] = o(\frac{1}{k})$ , it holds

$$\mathcal{L}(\hat{\theta}^*) \geq \mathbb{E}[\mathcal{L}(\theta_k)] - \frac{1}{2} \mathbb{E} \left[ \theta_k^\top \mathbf{F}(\hat{\theta}^*) \theta_k \right] - \eta \mu_k \|\mathbf{H}(\hat{\theta}^*) \hat{\theta}^*\|_\infty - \frac{1}{2} (\hat{\theta}^* - 2\theta_0)^\top \mathbf{H}(\hat{\theta}^*) \hat{\theta}^* + o \left( \frac{1}{k} \right).$$

Theorem 2 presents a lower bound of the minimum achievable training loss. Similar to the upper bound depicted in Theorem 4 in Appendix C, this bound relies on the local curvature of the loss landscape and the sample gradient. More precisely, a reduced minimum achievable training loss is attainable when the expected absolute sample gradients  $\mu_k$  and the FR norm  $\mathbb{E}[\theta_k^\top \mathbf{F}(\hat{\theta}^*) \theta_k]$  are high, or the expected current training loss  $\mathbb{E}[\mathcal{L}(\theta_k)]$  is low.

As an approximation of the Fisher [Schraudolph, 2002], the empirical Fisher information matrix (EFIM) is used, which is defined as  $\hat{\mathbf{F}}(\theta) = \frac{1}{N} \sum_{n=1}^N \frac{\partial}{\partial \theta} \ell(\theta; \mathbf{x}_n, \mathbf{y}_n) \frac{\partial}{\partial \theta} \ell(\theta; \mathbf{x}_n, \mathbf{y}_n)^\top$ .

### 3.4 Generalization Error

The decomposition of expected test loss (Eq. 3) underscores the significance of generalization error. The association of local flatness of the loss landscape with better generalization in DNNs has been widely embraced [Keskar et al., 2017, Wu et al., 2017, Yao et al., 2018, Liang et al., 2019]. This view was initially proposed by Hochreiter and Schmidhuber [1997] by showing that flat minima, requiring less information to characterize, should outperform sharp minima in terms of generalization.

In assessing flatness, most measurements approximate the local curvature of the loss landscape, characterizing flat minima as those with reduced Hessian eigenvalues [Wu et al., 2017]. As Hessians are very expensive to calculate, the sample gradient variance is used to measure local curvature properties. A rigorous discussion can be found in [Li et al., 2023, Section 3.2.2].

### 3.5 Zero-Shot Metric

Inspired by the theoretical insights, we propose SiGeo, jointly considering the minimum achievable training loss (estimated by the FR norm, average of absolute gradient estimates, and current training loss) and generalization error (estimated by sample variance of gradients). As Fig. 1b illustrated, the expected loss is proportional to the generalization error and minimum achievable training loss. The generalization error can be approximated by the gradient variance as discussed in Section 3.4 and the minimum achievable training loss can be approximated by absolute sample gradients, FR norm and current training loss, as depicted in Theorem 2. With experiments of different combinations and weights, we consider the following proxy formulation.

**Definition 1.** Let  $\theta^{(m)}$  denote the parameters of the  $m$ -th module, i.e.  $\theta^{(m)} \subseteq \theta$ . Let  $k$  denote the number of batches used to compute SiGeo. Given a neural network with  $M$  modules (containing trainable parameters), the zero-shot from information theory and geometry of loss landscape (SiGeo) is defined as follows:

$$SiGeo = \sum_{m=1}^M \lambda_1 \log \left( \left\| \boldsymbol{\mu}_k^{(m)} \oslash \boldsymbol{\sigma}_k^{(m)} \right\|_1 \right) + \lambda_2 \log \left( \boldsymbol{\theta}_k^\top \hat{\mathbf{F}}(\boldsymbol{\theta}_k) \boldsymbol{\theta}_k \right) - \lambda_3 \ell(\boldsymbol{\theta}_k; \mathcal{D}_k) \quad (7)$$

where  $\boldsymbol{\mu}_k^{(m)} = \frac{1}{k} \sum_{i=0}^k |\nabla_{\boldsymbol{\theta}^{(m)}} \ell(\boldsymbol{\theta}_i; \mathcal{D}_i)|$  is the average of absolute gradient estimate with respect to  $\boldsymbol{\theta}^{(m)}$  and  $\boldsymbol{\sigma}_k^{(m)} = \sqrt{\frac{1}{k} \sum_{i=0}^k \left( \nabla_{\boldsymbol{\theta}^{(m)}} \ell(\boldsymbol{\theta}_i; \mathcal{D}_i) - \frac{1}{k} \sum_{i=0}^k \nabla_{\boldsymbol{\theta}^{(m)}} \ell(\boldsymbol{\theta}_i; \mathcal{D}_i) \right)^2}$  is the standard deviation of gradient across batches. See Appendix E for the implementation details of SiGeo.

For the first term, we could consider a neuron-wise formulation  $\lambda_1 \log (\|\boldsymbol{\mu}_k \oslash \boldsymbol{\sigma}_k\|_1)$  as an alternative to the module-wise one, which is adapted from ZiCo. As depicted in Fig. 2, the second and third terms in Eq. 7 are important in utilizing the information accrued during the training process.

**Remark 2.** Based on our theoretical framework, various formulations for the zero-shot proxy can be chosen. In particular, when both  $\lambda_2$  and  $\lambda_3$  are set to zero, SiGeo simplifies to ZiCo. Likewise, if we allow for complete warming up of the supernet and fine-tuning of the subnet during the search, SiGeo becomes equivalent to one-shot NAS when  $\lambda_1$  and  $\lambda_2$  are set to zero. In practice, SiGeo reaches SOTA performance using just four batches (see Section 4). Thus, we compute SiGeo with only four input batches ( $k = 4$ ); this makes SiGeo computationally efficient.

## 4 Experiments

We conduct 5 sets of experiments: (1) Empirical validation of the theoretical findings (2) Evaluation of the SiGeo on zero-shot NAS benchmarks; (3) Evaluation of the SiGeo on NAS benchmarks under various warm-up levels; (4) Evaluation of SiGeo on click-through-rate (CTR) benchmark with various warm-up levels using the search space/policy and training setting from Zhang et al. [2023]; (5) Evaluation of SiGeo on CIFAR-10 and CIFAR-100 under the zero-shot setting using the same search space, search policy, and training settings from Lin et al. [2021a]. In addition, we have an ablation study to assess the efficacy of each key component of SiGeo in Appendix 4.5.

### 4.1 Setup

In Experiment (1), our primary goal is to validate Theorems 2. Notably, the sample variance of gradients has been extensively studied by Li et al. [2023] and thus we focus on the FR norm, the mean of absolute gradients and current training loss. To achieve this goal, we constructed two-layer MLP with rectified linear unit (ReLU) activation (MLP-ReLU) networks with varying hidden dimensions, ranging from 2 to 48 in increments of 2. Networks were trained on the MNIST dataset for 3 epochs using the SGD optimizer with a learning rate of 0.02. The batch size was set as 128.

In Experiment (2), we compare SiGeo with other zero-shot proxies on three NAS benchmarks, including (i) NAS-Bench-101 [Ying et al., 2019], a cell-based search space with 423,624 architectures, (ii) NAS-Bench-201 [Dong and Yang, 2020], consisting of 15,625 architectures, and (iii) NAS-Bench-301 [Zela et al., 2021], a surrogate benchmark for the DARTS search space [Liu et al., 2018], with  $10^{18}$  total architectures. Experiments are performed in the zero-shot setting.

In Experiment (3), we comprehensively compare our method against ZiCo under various warm-up levels on the same search spaces and tasks as used in Experiment (2).

In Experiment (4), we demonstrate empirical evaluations on three popular RecSys benchmarks for Click-Through Rates (CTR) prediction: Criteo<sup>2</sup>, Avazu<sup>3</sup> and KDD Cup 2012<sup>4</sup>. To identify the optimal child subnet within the NAS-Rec search space – encompassing NASRec Small and NASRec-Full [Zhang et al., 2023] – we employ the effective regularized evolution technique [Real et al., 2019]. All three datasets are pre-processed in the same fashion as AutoCTR [Song et al., 2020]. We conduct our experiments under three supernet warm-up levels: 0%, 1%, and 100%, corresponding to zero-shot, sub-one-shot and one-shot settings; see details in Appendix F.3.

In Experiment (5), we evaluate the compatibility of SiGeo on zero-shot NAS by utilizing the evaluation search algorithm and settings from ZiCo on CIFAR-10 and CIFAR-100 datasets [Krizhevsky et al., 2009]. Results and experiment settings are provided in Appendix H.

## 4.2 Empirical Justification for the Theory

Our empirical investigation starts with the validation of Theorem 2. The effectiveness of sample standard deviation of gradients (see Theorem 1) has been well validated by Li et al. [2023]. Therefore, we focus on the correlations between training loss and test loss in relation to the other three key statistics: (i) current training loss, (ii) FR norm, and (iii) mean absolute gradients. Specifically, we conduct assessments on three different warm-up levels, i.e. 0%, 10% and 40%. The concrete training configurations are described in Appendix F.1 and more results can be found in Appendix G.

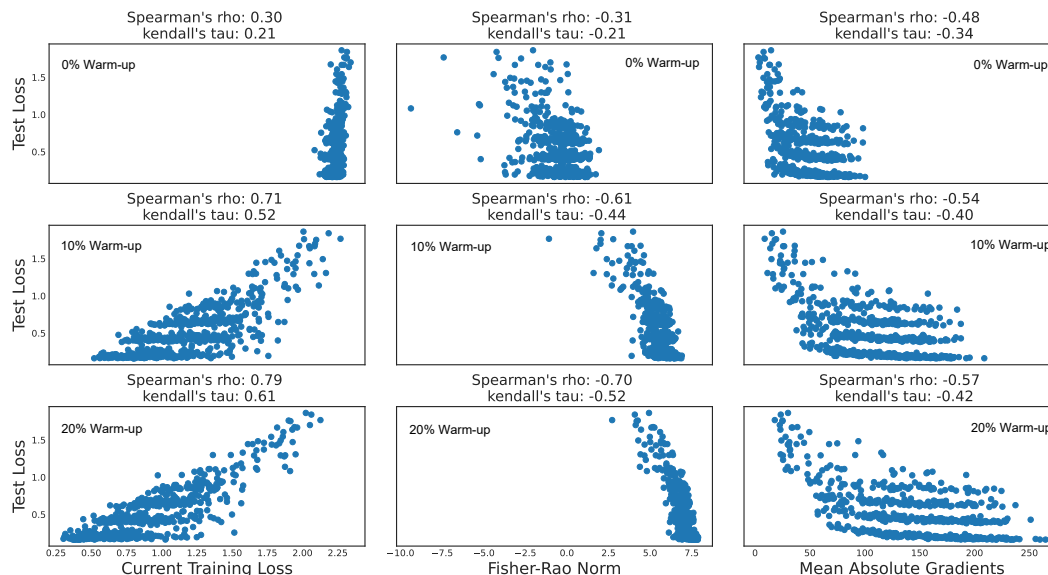


Figure 2: Test losses vs. statistics in Theorem 2. Results are generated by optimizing two-layer MLP-ReLU networks with varying hidden dimensions, ranging from 2 to 48 in increments of 2. The statistics for each network are computed after being warmed up with 0%, 10%, and 40% data.

Fig. 2 shows that networks with higher mean absolute gradients, FR norm values, or lower current training loss tend to have lower test and training loss. These results coincide with the conclusion drawn from Theorem 2. In addition, we observe a significant trend: as the warm-up level grows, there’s a marked improvement in the ranking correlation between the current training loss and the FR norm with the final training/test loss. In contrast, the correlation of the

<sup>2</sup><https://www.kaggle.com/competitions/criteo-display-ad-challenge/data>

<sup>3</sup><https://www.kaggle.com/competitions/avazu-ctr-prediction/data>

<sup>4</sup><https://www.kaggle.com/competitions/kddcup2012-track2/data>

mean absolute gradients remains fairly stable throughout this process. Given that the ZiCo proxy relies solely on the gradient standard deviation and the mean absolute gradients, the improved correlation coefficients of the FR norm and current training loss offer insights into why SiGeo outperforms the ZiCo method, particularly in the sub-one-shot setting.

### 4.3 Validating SiGeo in NAS benchmarks

We assess the performance of SiGeo under various warm-up levels. This validation takes place across a range of well-established computer vision tasks. It’s noteworthy that existing zero-shot methods predominantly focus their validation efforts on these tasks.

#### 4.3.1 Comparing SiGeo with Other Proxies under the Zero-Shot Setting

We compute the correlation coefficients between proxies and test accuracy on several datasets. Specifically, we use the CIFAR10 (CF10) dataset from NASBench-101 (NB101), NASBench-201 (NB201), and NASBench-301 (NB301); the CIFAR100 (CF100) dataset from NB201; and the ImageNet16-120 (IMGNT) dataset from NB201. As presented in Table 2, SiGeo demonstrates either the highest or equally high correlation with the true test accuracy compared to other zero-shot proxies. Note that experiments are conducted without warm-up of candidate architectures.

Table 2: The correlation coefficients between various zero-cost proxies and two naive proxies (#params and FLOPs) vs. test accuracy on various NAS benchmarks (Kendall and Spearman represent Kendall’s  $\tau$  and Spearman’s  $\rho$ , respectively). The best results are shown with bold fonts.

Proxy Name	NB101-CF10		NB201-CF10		NB201-CF100		NB201-IMGNT		NB301-CF10	
	Spearman	Kendall	Spearman	Kendall	Spearman	Kendall	Spearman	Kendall	Spearman	Kendall
epe-nas[Lopes et al., 2021]	0.00	0.00	0.70	0.52	0.60	0.43	0.33	0.23	0.00	0.00
fisher[Turner et al., 2020]	-0.28	-0.20	0.50	0.37	0.54	0.40	0.48	0.36	-0.28	-0.19
FLOPs [Ning et al., 2021]	0.36	0.25	0.69	0.50	0.71	0.52	0.67	0.48	0.42	0.29
grad-norm [Abdelfattah et al., 2021]	-0.25	-0.17	0.58	0.42	0.63	0.47	0.57	0.42	-0.04	-0.03
grasp[Wang et al., 2020b]	0.27	0.18	0.51	0.35	0.54	0.38	0.55	0.39	0.34	0.23
jacov [Mellor et al., 2021]	-0.29	-0.20	0.75	0.57	0.71	0.54	0.71	0.54	-0.04	-0.03
l2-norm [Abdelfattah et al., 2021]	0.50	0.35	0.68	0.49	0.72	0.52	0.69	0.50	0.45	0.31
NASWOT [Mellor et al., 2021]	0.31	0.21	0.77	0.58	0.80	0.62	0.77	0.59	0.47	0.32
#params [Ning et al., 2021]	0.37	0.25	0.72	0.54	0.73	0.55	0.69	0.52	0.46	0.31
plain [Abdelfattah et al., 2021]	-0.32	-0.22	-0.26	-0.18	-0.21	-0.14	-0.22	-0.15	-0.32	-0.22
snip [Lee et al., 2019]	-0.19	-0.14	0.58	0.43	0.63	0.47	0.57	0.42	-0.05	-0.03
synflow [Tanaka et al., 2020]	0.31	0.21	0.73	0.54	0.76	0.57	0.75	0.56	0.18	0.12
Zen [Lin et al., 2021b]	0.59	0.42	0.35	0.27	0.35	0.28	0.39	0.29	0.43	0.30
ZiCo [Li et al., 2023]	<b>0.63</b>	<b>0.46</b>	0.74	0.54	0.78	0.58	0.79	0.60	<b>0.50</b>	<b>0.35</b>
SiGeo (Ours)	<b>0.63</b>	<b>0.46</b>	<b>0.78</b>	<b>0.58</b>	<b>0.82</b>	<b>0.62</b>	<b>0.80</b>	<b>0.61</b>	<b>0.50</b>	<b>0.35</b>

#### 4.3.2 Comparing SiGeo with ZiCo on various Warm-up Levels

We conduct experiments to compare SiGeo against the SOTA proxy ZiCo under a sub-one-shot setting. Experiments are performed under the same setting of Section 4.3.1 with two key differences: (1) candidate architectures are warmed up before calculating the proxy scores; (2) we set  $\lambda_2 = 50$  and  $\lambda_3 = 1$  when the warm-up level is greater than zero. The results in Table 3 show (1) the ranking correlation of ZiCo does not improve much with more warm-up; (2) the ranking correlation of SiGeo improves significantly as the warm-up level increases. These results are consistent with the results in Section 4.2, underscoring the importance of the Fisher-Rao (FR) norm and current training loss in predicting the network performance when the candidate architectures are warmed up.

### 4.4 RecSys Benchmark Results

We use three RecSys benchmarks to validate the performance of SiGeo under different warm-up levels when compared with ZiCo and one-shot NAS approaches as well as hand-crafted models. Fig. 3 visualize the evaluation of our SiGeo-NAS against SOTA one-shot NAS baselines (DNAS[Krishna et al., 2021], PROFIT[Gao et al., 2021], AutoCTR[Song et al., 2020], NASRecNaet [Zhang et al., 2023]), and SOTA zero-shot NAS baseline (ZiCo [Li et al., 2023]) on three benchmark datasets: Criteo, Avazu, and KDD Cup 2012. All methods are trained in the NASRec-Full and NASRec-Small search spaces [Zhang et al., 2023]. The **detailed result** can be found in Table 5 of Appendix I.



Table 3: The correlation coefficients of SiGeo and ZiCo vs. test accuracy on various warm-up levels.

Benchmark		NB101-CF10		NB201-CF10		NB201-CF100		NB201-IMGNT		NB301-CF10	
Method	Warm-up Level	Spearman	Kendall	Spearman	Kendall	Spearman	Kendall	Spearman	Kendall	Spearman	Kendall
ZiCo	0%	0.63	0.46	0.74	0.54	0.78	0.58	0.79	0.60	0.5	0.35
ZiCo	10%	0.63	0.46	0.78	0.58	0.81	0.61	0.80	0.60	0.51	0.36
ZiCo	20%	0.64	0.46	0.77	0.57	0.81	0.62	0.79	0.59	0.51	0.36
ZiCo	40%	0.64	0.46	0.78	0.58	0.80	0.61	0.79	0.59	0.52	0.36
SiGeo	0%	0.63	0.46	0.78	0.58	0.82	0.62	0.80	0.61	0.5	0.35
SiGeo	10%	0.68	0.48	0.83	0.64	0.85	0.66	0.85	0.67	0.53	0.37
SiGeo	20%	0.69	0.51	0.84	0.65	0.87	0.69	0.86	0.68	0.55	0.40
SiGeo	40%	0.70	0.52	0.83	0.64	0.88	0.70	0.87	0.69	0.56	0.41

From Fig. 3, we observe that, after warming up the supernet using only 1% of the training data (sub-one-shot setting), SiGeo shows remarkable performance in comparison to established one-shot SOTA benchmarks with about 3X less computation time. In addition, when comparing SiGeo with hand-crafted CTR models [Guo et al., 2017, Lian et al., 2018, Naumov et al., 2019, Song et al., 2019] in Table 5, SiGeo-NAS demonstrates significantly improved performance.

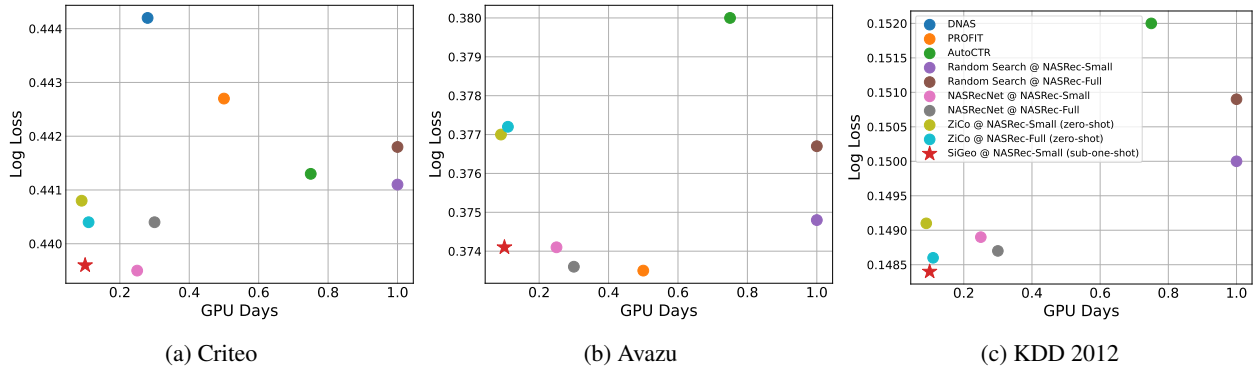


Figure 3: Performance of SiGeo-NAS on CTR Predictions Tasks. NASRec-Small and NASRec-Full are the two search spaces, and NASRecNet is the NAS method from Zhang et al. [2023].

#### 4.5 Ablation Study

To evaluate the effects of two key components, namely ZiCo and the FR norm, on SiGeo’s performance, we carried out an ablation study. Specifically, we compare the best subnets identified using ZiCo and the FR norm as proxies. All experiments are performed in a sub-one-shot setting with 1% warm-up, following the same configuration as outlined in Section 4.4. The top-15 models selected by each proxy are trained from scratch and their test accuracies are illustrated as boxplots in Fig. 4. The results reveal that the exclusion of any terms from SiGeo detrimentally affects performance.

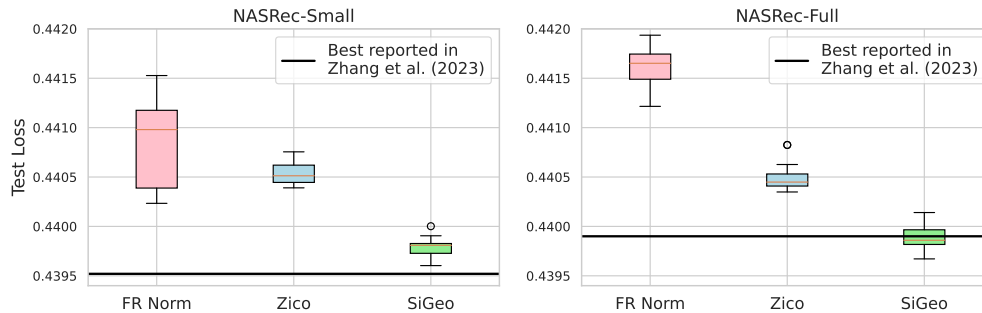


Figure 4: Evaluating the performance of two critical components (FR norm and ZiCo).

## 5 Conclusion

In this paper, we propose SiGeo, a new proxy proven to be increasingly effective when the candidate architectures continue to warm up. As the main theoretical contribution, we first present theoretical results that illuminate the connection between the minimum achievable test loss with the average of absolute gradient estimate, gradient standard deviation, FR norm, and the training loss under the sub-one-shot setting. Motivated by the theoretical insight, we have demonstrated that SiGeo achieves remarkable performance on three RecSys tasks (Criteo/Avazu/KDD-2012) with significantly lower search costs. In addition, we also validate SiGeo on various established NAS benchmarks (NASBench-101/NASBench-201/NASBench-301).

## References

- Hanxiao Liu, Karen Simonyan, and Yiming Yang. Darts: Differentiable architecture search. In *International Conference on Learning Representations (ICLR)*, 2018.
- Esteban Real, Sherry Moore, Andrew Selle, Saurabh Saxena, Yutaka Leon Suematsu, Jie Tan, Quoc V Le, and Alexey Kurakin. Large-scale evolution of image classifiers. In *International conference on machine learning*, pages 2902–2911. PMLR, 2017.
- Han Cai, Chuang Gan, Tianzhe Wang, Zhekai Zhang, and Song Han. Once for all: Train one network and specialize it for efficient deployment. In *International Conference on Learning Representations*, 2020. URL <https://arxiv.org/pdf/1908.09791.pdf>.
- Krishna Teja Chitty-Venkata, Murali Emani, Venkatram Vishwanath, and Arun K Somani. Neural architecture search for transformers: A survey. *IEEE Access*, 10:108374–108412, 2022.
- Igor Fedorov, Ramon Matas, Hokchhay Tann, Chuteng Zhou, Matthew Mattina, and Paul Whatmough. Udc: Unified dnas for compressible tinymml models for neural processing units. In S. Koyejo, S. Mohamed, A. Agarwal, D. Belgrave, K. Cho, and A. Oh, editors, *Advances in Neural Information Processing Systems*, volume 35, pages 18456–18471. Curran Associates, Inc., 2022. URL [https://proceedings.neurips.cc/paper\\_files/paper/2022/file/753d9584b57ba01a10482f1ea7734a89-Paper-Conference.pdf](https://proceedings.neurips.cc/paper_files/paper/2022/file/753d9584b57ba01a10482f1ea7734a89-Paper-Conference.pdf).
- Ravi Krishna, Aravind Kalaiah, Bichen Wu, Maxim Naumov, Dheevatsa Mudigere, Misha Smelyanskiy, and Kurt Keutzer. Differentiable nas framework and application to ads ctr prediction. *arXiv preprint arXiv:2110.14812*, 2021.
- Tunhou Zhang, Dehua Cheng, Yuchen He, Zhengxing Chen, Xiaoliang Dai, Liang Xiong, Feng Yan, Hai Li, Yiran Chen, and Wei Wen. Nasrec: Weight sharing neural architecture search for recommender systems. In *Proceedings of the ACM Web Conference 2023, WWW '23*, page 1199–1207, New York, NY, USA, 2023. Association for Computing Machinery. ISBN 9781450394161. doi: 10.1145/3543507.3583446. URL <https://doi.org/10.1145/3543507.3583446>.
- Qingquan Song, Dehua Cheng, Hanning Zhou, Jiyan Yang, Yuandong Tian, and Xia Hu. Towards automated neural interaction discovery for click-through rate prediction. In *Proceedings of the 26th ACM SIGKDD International Conference on Knowledge Discovery & Data Mining*, pages 945–955, 2020.
- Guihong Li, Yuedong Yang, Kartikeya Bhardwaj, and Radu Marculescu. Zico: Zero-shot NAS via inverse coefficient of variation on gradients. In *The Eleventh International Conference on Learning Representations*, 2023. URL <https://openreview.net/forum?id=rwo-ls5GqGn>.
- Colin White, Mikhail Khodak, Renbo Tu, Shital Shah, Sébastien Bubeck, and Debadeepta Dey. A deeper look at zero-cost proxies for lightweight nas. *ICLR Blog Track*, 2022.
- Chen Gao, Yinfeng Li, Quanming Yao, Depeng Jin, and Yong Li. Progressive feature interaction search for deep sparse network. In M. Ranzato, A. Beygelzimer, Y. Dauphin, P.S. Liang, and J. Wortman Vaughan, editors, *Advances in Neural Information Processing Systems*, volume 34, pages 392–403. Curran Associates, Inc., 2021. URL [https://proceedings.neurips.cc/paper\\_files/paper/2021/file/03b2ceb73723f8b53cd533e4fba898ee-Paper.pdf](https://proceedings.neurips.cc/paper_files/paper/2021/file/03b2ceb73723f8b53cd533e4fba898ee-Paper.pdf).
- Andrew Brock, Theo Lim, J.M. Ritchie, and Nick Weston. SMASH: One-shot model architecture search through hypernetworks. In *International Conference on Learning Representations*, 2018. URL <https://openreview.net/forum?id=rydeCEhs->.
- Xin Chen, Lingxi Xie, Jun Wu, and Qi Tian. Progressive differentiable architecture search: Bridging the depth gap between search and evaluation. In *Proceedings of the IEEE/CVF international conference on computer vision*, pages 1294–1303, 2019.

- Xuanyi Dong and Yi Yang. Searching for a robust neural architecture in four gpu hours. In *Proceedings of the IEEE/CVF Conference on Computer Vision and Pattern Recognition*, pages 1761–1770, 2019.
- Han Cai, Ligeng Zhu, and Song Han. ProxyllessNAS: Direct neural architecture search on target task and hardware. In *International Conference on Learning Representations*, 2019. URL <https://arxiv.org/pdf/1812.00332.pdf>.
- Dimitrios Stamoulis, Ruizhou Ding, Di Wang, Dimitrios Lymberopoulos, Bodhi Priyantha, Jie Liu, and Diana Marculescu. Single-path nas: Designing hardware-efficient convnets in less than 4 hours. In *Joint European Conference on Machine Learning and Knowledge Discovery in Databases*, pages 481–497. Springer, 2019.
- Changlin Li, Jiefeng Peng, Liuchun Yuan, Guangrun Wang, Xiaodan Liang, Liang Lin, and Xiaojun Chang. Block-wisely supervised neural architecture search with knowledge distillation. In *Proceedings of the IEEE/CVF Conference on Computer Vision and Pattern Recognition*, pages 1989–1998, 2020.
- Xiangxiang Chu, Bo Zhang, and Ruijun Xu. Fairnas: Rethinking evaluation fairness of weight sharing neural architecture search. In *Proceedings of the IEEE/CVF International Conference on computer vision*, pages 12239–12248, 2021.
- Zichao Guo, Xiangyu Zhang, Haoyuan Mu, Wen Heng, Zechun Liu, Yichen Wei, and Jian Sun. Single path one-shot neural architecture search with uniform sampling. In *Computer Vision—ECCV 2020: 16th European Conference, Glasgow, UK, August 23–28, 2020, Proceedings, Part XVI 16*, pages 544–560. Springer, 2020.
- Colby Banbury, Chuteng Zhou, Igor Fedorov, Ramon Matas, Urmish Thakker, Dibakar Gope, Vijay Janapa Reddi, Matthew Mattina, and Paul Whatmough. Micronets: Neural network architectures for deploying tinyml applications on commodity microcontrollers. *Proceedings of Machine Learning and Systems*, 3:517–532, 2021.
- David So, Quoc Le, and Chen Liang. The evolved transformer. In *International conference on machine learning*, pages 5877–5886. PMLR, 2019.
- Hanrui Wang, Zhanghao Wu, Zhijian Liu, Han Cai, Ligeng Zhu, Chuang Gan, and Song Han. Hat: Hardware-aware transformers for efficient natural language processing. *arXiv preprint arXiv:2005.14187*, 2020a.
- Joe Mellor, Jack Turner, Amos Storkey, and Elliot J Crowley. Neural architecture search without training. In *International Conference on Machine Learning*, pages 7588–7598. PMLR, 2021.
- Wuyang Chen, Xinyu Gong, and Zhangyang Wang. Neural architecture search on imagenet in four gpu hours: A theoretically inspired perspective. In *International Conference on Learning Representations*, 2021.
- Kartikeya Bhardwaj, James Ward, Caleb Tung, Dibakar Gope, Lingchuan Meng, Igor Fedorov, Alex Chalfin, Paul Whatmough, and Danny Loh. Restructurable activation networks. *arXiv preprint arXiv:2208.08562*, 2022.
- Ming Lin, Pichao Wang, Zhenhong Sun, Heseng Chen, Xiuyu Sun, Qi Qian, Hao Li, and Rong Jin. Zen-nas: A zero-shot nas for high-performance image recognition. In *Proceedings of the IEEE/CVF International Conference on Computer Vision*, pages 347–356, 2021a.
- Mohamed S. Abdelfattah, Abhinav Mehrotra, Łukasz Dudziak, and Nicholas D. Lane. Zero-Cost Proxies for Lightweight NAS. In *International Conference on Learning Representations (ICLR)*, 2021.
- Namhoon Lee, Thalaisyasingam Ajanthan, and Philip H. S. Torr. Snip: single-shot network pruning based on connection sensitivity. In *7th International Conference on Learning Representations, ICLR 2019, New Orleans, LA, USA, May 6-9, 2019*. OpenReview.net, 2019. URL <https://openreview.net/forum?id=B1VZqjAcYX>.
- Hidenori Tanaka, Daniel Kunin, Daniel L Yamins, and Surya Ganguli. Pruning neural networks without any data by iteratively conserving synaptic flow. In H. Larochelle, M. Ranzato, R. Hadsell, M.F. Balcan, and H. Lin, editors, *Advances in Neural Information Processing Systems*, volume 33, pages 6377–6389. Curran Associates, Inc., 2020. URL [https://proceedings.neurips.cc/paper\\_files/paper/2020/file/46a4378f835dc8040c8057beb6a2da52-Paper.pdf](https://proceedings.neurips.cc/paper_files/paper/2020/file/46a4378f835dc8040c8057beb6a2da52-Paper.pdf).
- Chaoqi Wang, Guodong Zhang, and Roger Grosse. Picking winning tickets before training by preserving gradient flow. In *International Conference on Learning Representations*, 2020b. URL <https://openreview.net/forum?id=SkgsACVKPH>.
- Vasco Lopes, Saeid Alirezazadeh, and Luís A Alexandre. Epe-nas: Efficient performance estimation without training for neural architecture search. In *International Conference on Artificial Neural Networks*, pages 552–563. Springer, 2021.
- Haibin Wang, Ce Ge, Heseng Chen, and Xiuyu Sun. Prenas: Preferred one-shot learning towards efficient neural architecture search. In *International Conference on Machine Learning (ICML)*, July 2023.

- Chengyue Gong, Dilin Wang, Meng Li, Xinlei Chen, Zhicheng Yan, Yuandong Tian, Vikas Chandra, et al. Nasvit: Neural architecture search for efficient vision transformers with gradient conflict aware supernet training. In *International Conference on Learning Representations*, 2021.
- Valentin Thomas, Fabian Pedregosa, Bart Merriënboer, Pierre-Antoine Manzagol, Yoshua Bengio, and Nicolas Le Roux. On the interplay between noise and curvature and its effect on optimization and generalization. In *International Conference on Artificial Intelligence and Statistics*, pages 3503–3513. PMLR, 2020.
- Byung-Kwan Lee, Junho Kim, and Yong Man Ro. Masking adversarial damage: Finding adversarial saliency for robust and sparse network. In *Proceedings of the IEEE/CVF Conference on Computer Vision and Pattern Recognition (CVPR)*, pages 15126–15136, June 2022.
- Ryo Karakida, Shotaro Akaho, and Shun-ichi Amari. Universal statistics of fisher information in deep neural networks: Mean field approach. In *The 22nd International Conference on Artificial Intelligence and Statistics*, pages 1032–1041. PMLR, 2019.
- Tengyuan Liang, Tomaso Poggio, Alexander Rakhlin, and James Stokes. Fisher-rao metric, geometry, and complexity of neural networks. In *The 22nd international conference on artificial intelligence and statistics*, pages 888–896. PMLR, 2019.
- Cong Fang, Zhouchen Lin, and Tong Zhang. Sharp analysis for nonconvex sgd escaping from saddle points. In *Conference on Learning Theory*, pages 1192–1234. PMLR, 2019.
- Bobby Kleinberg, Yuanzhi Li, and Yang Yuan. An alternative view: When does sgd escape local minima? In *International conference on machine learning*, pages 2698–2707. PMLR, 2018.
- Yi Xu, Rong Jin, and Tianbao Yang. First-order stochastic algorithms for escaping from saddle points in almost linear time. In S. Bengio, H. Wallach, H. Larochelle, K. Grauman, N. Cesa-Bianchi, and R. Garnett, editors, *Advances in Neural Information Processing Systems*, volume 31. Curran Associates, Inc., 2018. URL [https://proceedings.neurips.cc/paper\\_files/paper/2018/file/217e342fc01668b10cb1188d40d3370e-Paper.pdf](https://proceedings.neurips.cc/paper_files/paper/2018/file/217e342fc01668b10cb1188d40d3370e-Paper.pdf).
- James Martens. New insights and perspectives on the natural gradient method. *The Journal of Machine Learning Research*, 21(1):5776–5851, 2020.
- Guillaume Garrigos and Robert M Gower. Handbook of convergence theorems for (stochastic) gradient methods. *arXiv preprint arXiv:2301.11235*, 2023.
- Simon Lacoste-Julien, Mark Schmidt, and Francis Bach. A simpler approach to obtaining an  $o(1/t)$  convergence rate for the projected stochastic subgradient method. *arXiv preprint arXiv:1212.2002*, 2012.
- Léon Bottou and Yann Le Cun. On-line learning for very large data sets. *Applied stochastic models in business and industry*, 21(2):137–151, 2005.
- Nicol N Schraudolph. Fast curvature matrix-vector products for second-order gradient descent. *Neural computation*, 14(7):1723–1738, 2002.
- Nitish Shirish Keskar, Dheevatsa Mudigere, Jorge Nocedal, Mikhail Smelyanskiy, and Ping Tak Peter Tang. On large-batch training for deep learning: Generalization gap and sharp minima. In *5th International Conference on Learning Representations, ICLR 2017, Toulon, France, April 24-26, 2017, Conference Track Proceedings*. OpenReview.net, 2017. URL <https://openreview.net/forum?id=H1oyRlYgg>.
- Lei Wu, Zhanxing Zhu, et al. Towards understanding generalization of deep learning: Perspective of loss landscapes. *arXiv preprint arXiv:1706.10239*, 2017.
- Zhewei Yao, Amir Gholami, Qi Lei, Kurt Keutzer, and Michael W Mahoney. Hessian-based analysis of large batch training and robustness to adversaries. In S. Bengio, H. Wallach, H. Larochelle, K. Grauman, N. Cesa-Bianchi, and R. Garnett, editors, *Advances in Neural Information Processing Systems*, volume 31. Curran Associates, Inc., 2018. URL [https://proceedings.neurips.cc/paper\\_files/paper/2018/file/102f0bb6efb3a6128a3c750dd16729be-Paper.pdf](https://proceedings.neurips.cc/paper_files/paper/2018/file/102f0bb6efb3a6128a3c750dd16729be-Paper.pdf).
- Sepp Hochreiter and Jürgen Schmidhuber. Flat minima. *Neural computation*, 9(1):1–42, 1997.
- Chris Ying, Aaron Klein, Eric Christiansen, Esteban Real, Kevin Murphy, and Frank Hutter. Nas-bench-101: Towards reproducible neural architecture search. In *International conference on machine learning*, pages 7105–7114. PMLR, 2019.
- Xuanyi Dong and Yi Yang. Nas-bench-201: Extending the scope of reproducible neural architecture search. In *International Conference on Learning Representations (ICLR)*, 2020. URL <https://openreview.net/forum?id=HJxyZkBKDr>.

- Arber Zela, Julien Siems, Lucas Zimmer, Jovita Lukasik, Margret Keuper, and Frank Hutter. Surrogate nas benchmarks: Going beyond the limited search spaces of tabular nas benchmarks. In *International Conference on Learning Representations*, 2021.
- Esteban Real, Alok Aggarwal, Yanping Huang, and Quoc V. Le. Regularized evolution for image classifier architecture search. In *Proceedings of the Thirty-Third AAAI Conference on Artificial Intelligence and Thirty-First Innovative Applications of Artificial Intelligence Conference and Ninth AAAI Symposium on Educational Advances in Artificial Intelligence*, AAAI’19/IAAI’19/EAAI’19. AAAI Press, 2019. ISBN 978-1-57735-809-1. doi: 10.1609/aaai.v33i01.33014780. URL <https://doi.org/10.1609/aaai.v33i01.33014780>.
- Alex Krizhevsky, Geoffrey Hinton, et al. Learning multiple layers of features from tiny images, 2009.
- Jack Turner, Elliot J. Crowley, Michael O’Boyle, Amos Storkey, and Gavin Gray. Blockswap: Fisher-guided block substitution for network compression on a budget. In *International Conference on Learning Representations*, 2020. URL <https://openreview.net/forum?id=Sk1kDkSFpB>.
- Xuefei Ning, Changcheng Tang, Wenshuo Li, Zixuan Zhou, Shuang Liang, Huazhong Yang, and Yu Wang. Evaluating efficient performance estimators of neural architectures. In M. Ranzato, A. Beygelzimer, Y. Dauphin, P.S. Liang, and J. Wortman Vaughan, editors, *Advances in Neural Information Processing Systems*, volume 34, pages 12265–12277. Curran Associates, Inc., 2021. URL [https://proceedings.neurips.cc/paper\\_files/paper/2021/file/65d90fc6d307590b14e9e1800d4e8eab-Paper.pdf](https://proceedings.neurips.cc/paper_files/paper/2021/file/65d90fc6d307590b14e9e1800d4e8eab-Paper.pdf).
- Ming Lin, Pichao Wang, Zhenhong Sun, Heseng Chen, Xiuyu Sun, Qi Qian, Hao Li, and Rong Jin. Zen-nas: A zero-shot nas for high-performance deep image recognition. In *2021 IEEE/CVF International Conference on Computer Vision, ICCV 2021*, 2021b.
- Huifeng Guo, Ruiming Tang, Yunming Ye, Zhenguo Li, and Xiuqiang He. Deepfm: A factorization-machine based neural network for CTR prediction. In Carles Sierra, editor, *Proceedings of the Twenty-Sixth International Joint Conference on Artificial Intelligence, IJCAI 2017, Melbourne, Australia, August 19-25, 2017*, pages 1725–1731. ijcai.org, 2017. doi: 10.24963/ijcai.2017/239. URL <https://doi.org/10.24963/ijcai.2017/239>.
- Jianxun Lian, Xiaohuan Zhou, Fuzheng Zhang, Zhongxia Chen, Xing Xie, and Guangzhong Sun. xdeepfm: Combining explicit and implicit feature interactions for recommender systems. In *Proceedings of the 24th ACM SIGKDD international conference on knowledge discovery & data mining*, pages 1754–1763, 2018.
- Maxim Naumov, Dheevatsa Mudigere, Hao-Jun Michael Shi, Jianyu Huang, Narayanan Sundaraman, Jongsoo Park, Xiaodong Wang, Udit Gupta, Carole-Jean Wu, Alisson G Azzolini, et al. Deep learning recommendation model for personalization and recommendation systems. *arXiv preprint arXiv:1906.00091*, 2019.
- Weiping Song, Chence Shi, Zhiping Xiao, Zhijian Duan, Yewen Xu, Ming Zhang, and Jian Tang. AutoInt: Automatic feature interaction learning via self-attentive neural networks. In *Proceedings of the 28th ACM international conference on information and knowledge management*, pages 1161–1170, 2019.
- Shun-Ichi Amari. Natural gradient works efficiently in learning. *Neural computation*, 10(2):251–276, 1998.
- Eric Moulines and Francis Bach. Non-asymptotic analysis of stochastic approximation algorithms for machine learning. In J. Shawe-Taylor, R. Zemel, P. Bartlett, F. Pereira, and K.Q. Weinberger, editors, *Advances in Neural Information Processing Systems*, volume 24. Curran Associates, Inc., 2011. URL [https://proceedings.neurips.cc/paper\\_files/paper/2011/file/40008b9a5380fcacce3976bf7c08af5b-Paper.pdf](https://proceedings.neurips.cc/paper_files/paper/2011/file/40008b9a5380fcacce3976bf7c08af5b-Paper.pdf).
- Axel Ruhe. Perturbation bounds for means of eigenvalues and invariant subspaces. *BIT Numerical Mathematics*, 10(3):343–354, 1970.
- Zhaojun Bai and Gene H Golub. Bounds for the trace of the inverse and the determinant of symmetric positive definite matrices. *Annals of Numerical Mathematics*, 4:29–38, 1996.
- Arjun Krishnakumar, Colin White, Arber Zela, Renbo Tu, Mahmoud Safari, and Frank Hutter. Nas-bench-suite-zero: Accelerating research on zero cost proxies. In S. Koyejo, S. Mohamed, A. Agarwal, D. Belgrave, K. Cho, and A. Oh, editors, *Advances in Neural Information Processing Systems*, volume 35, pages 28037–28051. Curran Associates, Inc., 2022. URL [https://proceedings.neurips.cc/paper\\_files/paper/2022/file/b3835dd49b7d5bb062aecccc14d8a675-Paper-Datasets\\_and\\_Benchmarks.pdf](https://proceedings.neurips.cc/paper_files/paper/2022/file/b3835dd49b7d5bb062aecccc14d8a675-Paper-Datasets_and_Benchmarks.pdf).
- Hieu Pham, Melody Guan, Barret Zoph, Quoc Le, and Jeff Dean. Efficient neural architecture search via parameters sharing. In *International conference on machine learning*, pages 4095–4104. PMLR, 2018.
- Hongyi Zhang, Moustapha Cissé, Yann N. Dauphin, and David Lopez-Paz. mixup: Beyond empirical risk minimization. In *6th International Conference on Learning Representations, ICLR 2018, Vancouver, BC, Canada, April 30 - May 3, 2018, Conference Track Proceedings*. OpenReview.net, 2018. URL <https://openreview.net/forum?id=r1Ddp1-Rb>.

- Christian Szegedy, Vincent Vanhoucke, Sergey Ioffe, Jon Shlens, and Zbigniew Wojna. Rethinking the inception architecture for computer vision. In *Proceedings of the IEEE conference on computer vision and pattern recognition*, pages 2818–2826, 2016.
- Zhun Zhong, Liang Zheng, Guoliang Kang, Shaozi Li, and Yi Yang. Random erasing data augmentation. In *Proceedings of the AAAI conference on artificial intelligence*, volume 34, pages 13001–13008, 2020.
- Ekin D Cubuk, Barret Zoph, Dandelion Mane, Vijay Vasudevan, and Quoc V Le. Autoaugment: Learning augmentation strategies from data. In *Proceedings of the IEEE/CVF conference on computer vision and pattern recognition*, pages 113–123, Los Alamitos, CA, USA, jun 2019. IEEE Computer Society. doi: 10.1109/CVPR.2019.00020.
- Ilya Loshchilov and Frank Hutter. SGDR: stochastic gradient descent with warm restarts. In *5th International Conference on Learning Representations, ICLR 2017, Toulon, France, April 24-26, 2017, Conference Track Proceedings*. OpenReview.net, 2017. URL <https://openreview.net/forum?id=Skq89Scxx>.
- Gustavo Aguilar, Yuan Ling, Yu Zhang, Benjamin Yao, Xing Fan, and Chenlei Guo. Knowledge distillation from internal representations. In *Proceedings of the AAAI Conference on Artificial Intelligence*, volume 34, pages 7350–7357, 2020.
- Kaiming He, Xiangyu Zhang, Shaoqing Ren, and Jian Sun. Deep residual learning for image recognition. In *Proceedings of the IEEE conference on computer vision and pattern recognition*, pages 770–778, 2016.
- Ilija Radosavovic, Raj Prateek Kosaraju, Ross Girshick, Kaiming He, and Piotr Dollár. Designing network design spaces. In *Proceedings of the IEEE/CVF conference on computer vision and pattern recognition*, pages 10428–10436, 2020.

## A Assumption Justification

The assumption **A.1** is originally proposed by Amari [1998] to show the Fisher efficiency result. This assumption has been widely used by many studies [Lee et al., 2022, Karakida et al., 2019, Thomas et al., 2020] to suggest that the model is powerful enough to capture the training distribution at  $\theta = \hat{\theta}^*$ . We emphasize that Assumption **A.1** serves solely as a theoretical justification for substituting the Hessian matrix with the Fisher Information Matrix. Even in cases where this assumption fails to hold, the study by Thomas et al. [2020] has shown that the matrices tend to converge as the model training progresses.

The assumption for the initiation of supernet **A.2** holds importance in our theoretical analysis. This assumption aligns with recent theoretical findings for SGD. Specifically, after the warm-up phase, where the supernet is trained using a limited subset of the training data, the weights of the supernet are expected to escape the saddle points, settling near a specific local minimum [Fang et al., 2019, Kleinberg et al., 2018, Xu et al., 2018]. In practice, this assumption is readily attainable: If **A.2** doesn't hold, one can simply introduce more samples to adequately warm up the supernet. In addition, we also observe that for numerous tasks, particularly those in the realm of computer vision, achieving satisfactory performance doesn't necessarily require warming up the supernet.

In most deep learning literature, the almost everywhere differentiability assumption **A.3** typically holds due to the need to calculate the gradient.

Lastly, **A.4** is the regularity condition that provides a foundational basis for performing mathematical operations that rely on the existence of the inverse of these matrices. In addition, this assumption directly implies the convexity of the loss function in the space  $\mathbb{B}$ .

## B Proof of Theorem 1

**Lemma 1.** Assume **A.4**. If  $\ell$  is differentiable, for any  $(\mathbf{x}, \mathbf{y}) \in \mathcal{X} \times \mathcal{Y}$ , it holds

$$\ell(\theta_1) \geq \ell(\theta_2) + \langle \nabla \ell(\theta_2; \mathbf{x}, \mathbf{y}), \theta_1 - \theta_2 \rangle, \text{ for all } \theta_1, \theta_2 \in \mathbb{B}$$

*Proof.* The positive definite Hessian in Assumption **A.4** directly implies the convexity of loss function  $\ell$  with respect to  $\theta$  for all  $(\mathbf{x}, \mathbf{y}) \in \mathcal{X} \times \mathcal{Y}$ . Then the conclusion immediately follow Garrigos and Gower [2023, Lemma 2.8].  $\square$

**Theorem 1.** Assume **A.1-A.4**. Consider  $\{\theta_k\}_{k \in \mathbb{Z}}$  a sequence generated by the first-order (SGD) algorithm (4), with a decreasing sequence of stepsizes satisfying  $\eta_k > 0$ . Let  $\sigma_k^2 := \text{Var}[\nabla \ell(\theta_k; \mathcal{D}_k)]$  denote the variance of sample gradient, where the variance is taken over the joint distribution of all the training samples until the  $k$ -th iteration (also known as filtration in stochastic approximation literature). Then It holds that

$$\mathbb{E}[\mathcal{L}(\bar{\theta}_k)] - \mathcal{L}(\hat{\theta}^*) \leq \frac{\|\theta_0 - \hat{\theta}^*\|}{2 \sum_{t=0}^{k-1} \eta_t} + \frac{1}{2} \sum_{i=0}^{k-1} \sigma_i^2$$

*Proof.* For a given weight  $\theta_k$ , the sample gradient estimate is an unbiased estimate of expected gradient, i.e.  $\mathbb{E}[\nabla \ell(\theta_k; \mathcal{D}_k) | \theta_k] = \mathbb{E}[\frac{1}{|\mathcal{D}_k|} \sum_{(\mathbf{x}_n, \mathbf{y}_n) \in \mathcal{D}_k} \nabla \ell(\theta_k; \mathbf{x}_n, \mathbf{y}_n) | \theta_k] = \nabla \mathcal{L}(\theta_k)$  under some mild conditions. We will note  $\mathbb{E}_k[\cdot]$  instead of  $\mathbb{E}[\cdot | \theta_k]$ , and  $\text{Var}_k[\cdot]$  instead of  $\text{Var}[\cdot | \theta_k]$ , for simplicity. Thus, we have the gradient variance

$$\text{Var}_k[\nabla \ell(\theta_k; \mathcal{D}_k)] = \mathbb{E}_k[\|\nabla \ell(\theta_k; \mathcal{D}_k)\|^2] - \|\mathbb{E}_k[\nabla \ell(\theta_k; \mathcal{D}_k)]\|^2 = \mathbb{E}_k[\|\nabla \ell(\theta_k; \mathcal{D}_k)\|^2]. \quad (8)$$

Let us start by analyzing the behavior of  $\|\theta_k - \hat{\theta}^*\|^2$ . By expanding the squares, we obtain

$$\|\theta_{k+1} - \hat{\theta}^*\|^2 = \|\theta_k - \hat{\theta}^*\|^2 - 2\eta_k \langle \nabla \ell(\theta_k; \mathcal{D}_k), \theta_k - \hat{\theta}^* \rangle + \eta_k^2 \|\nabla \ell(\theta_k; \mathcal{D}_k)\|^2$$

Hence, after taking the expectation conditioned on  $\theta_k$ , we can use the convexity of  $\ell$  to obtain:

$$\begin{aligned} \mathbb{E}_k[\|\theta_{k+1} - \hat{\theta}^*\|^2] &= \|\theta_k - \hat{\theta}^*\|^2 - 2\eta_k \langle \mathbb{E}_k[\nabla \ell(\theta_k; \mathcal{D}_k)], \theta_k - \hat{\theta}^* \rangle + \eta_k^2 \mathbb{E}_k[\|\nabla \ell(\theta_k; \mathcal{D}_k)\|^2] \\ &\leq \|\theta_k - \hat{\theta}^*\|^2 + 2\eta_k \langle \nabla \mathcal{L}(\theta_k), \theta_k - \hat{\theta}^* \rangle + \eta_k^2 \mathbb{E}_k[\|\nabla \ell(\theta_k; \mathcal{D}_k)\|^2] \\ &\leq \|\theta_k - \hat{\theta}^*\|^2 + 2\eta_k (\mathcal{L}(\theta_k) - \mathcal{L}(\hat{\theta}^*)) + \eta_k^2 \text{Var}_k[\nabla \ell(\theta_k; \mathcal{D}_k)] \end{aligned} \quad (9)$$

where the last equation holds due to Lemma 1 and Eq. (8). Rearranging and taking the full expectation of Eq. (9) over all past training samples until iteration  $k$ , we have

$$2\eta_k (\mathbb{E}[\mathcal{L}(\boldsymbol{\theta}_k)] - \mathcal{L}(\boldsymbol{\theta}^*)) \leq \mathbb{E}[\|\boldsymbol{\theta}_k - \hat{\boldsymbol{\theta}}^*\|] - \mathbb{E}[\|\boldsymbol{\theta}_{k+1} - \hat{\boldsymbol{\theta}}^*\|] + \eta_k^2 \mathbb{E}[\text{Var}_k[\nabla\ell(\boldsymbol{\theta}_k; \mathcal{D}_k)]] \quad (10)$$

Due to law of total variance, it holds

$$\sigma^2 = \text{Var}[\nabla\ell(\boldsymbol{\theta}_k; \mathcal{D}_k)] = \mathbb{E}[\text{Var}[\nabla\ell(\boldsymbol{\theta}_k; \mathcal{D}_k|\boldsymbol{\theta}_k)]] + \text{Var}[\mathbb{E}[\nabla\ell(\boldsymbol{\theta}_k; \mathcal{D}_k)|\boldsymbol{\theta}_k]] \geq \mathbb{E}[\text{Var}_k[\nabla\ell(\boldsymbol{\theta}_k; \mathcal{D}_k)]] .$$

Then Eq. 10 becomes

$$2\eta_k (\mathbb{E}[\mathcal{L}(\boldsymbol{\theta}_k)] - \mathcal{L}(\boldsymbol{\theta}^*)) \leq \mathbb{E}[\|\boldsymbol{\theta}_k - \hat{\boldsymbol{\theta}}^*\|] - \mathbb{E}[\|\boldsymbol{\theta}_{k+1} - \hat{\boldsymbol{\theta}}^*\|] + \eta_k^2 \sigma^2$$

Summing over  $i = 0, 1, \dots, k-1$  and using telescopic cancellation gives

$$2 \sum_{i=0}^{k-1} \eta_i (\mathbb{E}[\mathcal{L}(\boldsymbol{\theta}_i)] - \mathcal{L}(\boldsymbol{\theta}^*)) \leq \|\boldsymbol{\theta}_0 - \hat{\boldsymbol{\theta}}^*\| - \mathbb{E}[\|\boldsymbol{\theta}_k - \hat{\boldsymbol{\theta}}^*\|] + \sum_{i=0}^{k-1} \eta_i^2 \sigma^2$$

Since  $\mathbb{E}[\|\boldsymbol{\theta}_k - \hat{\boldsymbol{\theta}}^*\|] \geq 0$ , dividing both sides by  $2 \sum_{t=0}^{k-1} \eta_t$  gives:

$$\sum_{i=0}^{k-1} \frac{\eta_i}{\sum_{t=0}^{k-1} \eta_t} (\mathbb{E}[\mathcal{L}(\boldsymbol{\theta}_i)] - \mathcal{L}(\boldsymbol{\theta}^*)) \leq \frac{\|\boldsymbol{\theta}_0 - \hat{\boldsymbol{\theta}}^*\|}{2 \sum_{t=0}^{k-1} \eta_t} + \sum_{i=0}^{k-1} \frac{\eta_i^2}{2 \sum_{t=0}^{k-1} \eta_t} \sigma^2$$

Define for  $i = 0, 1, \dots, k-1$

$$p_{k,i} := \frac{\eta_i^2}{\sum_{t=0}^{k-1} \eta_t}$$

and observe that  $p_{k,i} \geq 0$  and  $\sum_{i=0}^{k-1} p_{k,i} = 1$ . This allows us to treat the  $\{p_{k,i}\}$  as probabilities. Then using the fact that  $\ell$  is convex together with Jensen's inequality gives

$$\begin{aligned} \mathbb{E}[\mathcal{L}(\bar{\boldsymbol{\theta}}_k)] - \mathcal{L}(\hat{\boldsymbol{\theta}}^*) &\leq \sum_{i=0}^{k-1} \frac{\eta_i}{\sum_{t=0}^{k-1} \eta_t} (\mathbb{E}[\mathcal{L}(\boldsymbol{\theta}_i)] - \mathcal{L}(\boldsymbol{\theta}^*)) \\ &\leq \frac{\|\boldsymbol{\theta}_0 - \hat{\boldsymbol{\theta}}^*\|}{2 \sum_{t=0}^{k-1} \eta_t} + \sum_{i=0}^{k-1} \frac{\eta_i^2}{2 \sum_{t=0}^{k-1} \eta_t} \text{Var}[\nabla\ell(\boldsymbol{\theta}_i; \mathcal{D}_i)] \\ &\leq \frac{\|\boldsymbol{\theta}_0 - \hat{\boldsymbol{\theta}}^*\|}{2 \sum_{t=0}^{k-1} \eta_t} + \frac{1}{2} \sum_{i=0}^{k-1} \sigma_k^2 \end{aligned} \quad (11)$$

where the last inequality holds because  $p_{k,i} \leq 1$ . □

## C Convergence Analysis with Strong Convexity Assumption

In this section, we will extend our analysis to strong convex loss function, a stronger assumption than convexity. Mathematically, we assume that the expected loss function of candidate network  $\mathcal{L}(\boldsymbol{\theta})$  is locally strongly convex with convexity constant  $M$ , that is,  $\mathcal{L}(\boldsymbol{\theta}_1) \geq \mathcal{L}(\boldsymbol{\theta}_2) + \langle \nabla\mathcal{L}(\boldsymbol{\theta}_2), \boldsymbol{\theta}_1 - \boldsymbol{\theta}_2 \rangle + \frac{M}{2} \|\boldsymbol{\theta}_1 - \boldsymbol{\theta}_2\|^2$  for any  $\boldsymbol{\theta}_1, \boldsymbol{\theta}_2 \in \mathbb{B}$ .

In addition, we define the covariance matrix of gradient

$$\mathbf{C} = \mathbb{E} \left[ \left( \nabla\ell(\hat{\boldsymbol{\theta}}^*; \mathbf{x}, \mathbf{y}) - \mathbb{E}[\nabla\ell(\hat{\boldsymbol{\theta}}^*; \mathbf{x}, \mathbf{y})] \right) \left( \nabla\ell(\hat{\boldsymbol{\theta}}^*; \mathbf{x}, \mathbf{y}) - \mathbb{E}[\nabla\ell(\hat{\boldsymbol{\theta}}^*; \mathbf{x}, \mathbf{y})] \right)^\top \right].$$

Subsequently, the variance of sample gradient is denoted by  $\text{Tr}(\mathbf{C}) = \text{Var}[\nabla\ell(\hat{\boldsymbol{\theta}}^*; \mathbf{x}, \mathbf{y})]$ .

Based on the strong convexity assumption, the first theorem is established by using a result from Moulines and Bach [2011]; see the proof in Appendix C.1.



**Theorem 3.** *Assume A.1-A.4. If the loss function is strongly convex, under the regularity conditions in Moulines and Bach [2011], for the average iterate  $\bar{\theta}_k = \frac{1}{k+1} \sum_{i=0}^k \theta_i$  with a first-order SGD (4) ( $\mathbf{B}_k = \mathbf{I}$ ), it holds*

$$\mathbb{E}[\ell(\bar{\theta}_k; \mathbf{x}, \mathbf{y}) - \ell(\hat{\theta}^*; \mathbf{x}, \mathbf{y})] \leq L \mathbb{E}[\|\bar{\theta}_k - \hat{\theta}^*\|^2]^{1/2} \leq \mathcal{O}\left(\frac{\text{Tr}(\mathbf{F}(\hat{\theta}^*)^{-1}) \sqrt{\text{Tr}(\mathbf{C})}}{\sqrt{k+1}}\right) + o\left(\frac{1}{\sqrt{k+1}}\right)$$

Then we present our main theorem which relates the optimality gap with FR norm and standard deviation values. The proof of the following theorem can be found in Appendix C.2.

**Theorem 4.** *Assume A.1-A.4. Consider the first order SGD update 4 ( $\mathbf{B}_k = \mathbf{I}$ ) with fixed learning rate  $\eta$ . If the loss function is strongly convex, under the same assumption as stated in Lemma 3, the expected loss is bounded as follows*

$$\mathbb{E}[\ell(\bar{\theta}_k; \mathbf{x}, \mathbf{y})] - \mathbb{E}[\ell(\hat{\theta}^*; \mathbf{x}, \mathbf{y})] \leq \mathcal{O}\left(\frac{\sqrt{\text{Tr}(\mathbf{C})}}{2\sqrt{k+1}} \left[ \frac{d^2 M}{\mathbb{E}[\theta_k^T \mathbf{F}(\hat{\theta}^*) \theta_k] + 2\eta \mathbb{E}[\sum_{i=0}^k \nabla \ell(\theta_i; \mathcal{D}_i)]^T \mathbf{F}(\hat{\theta}^*) \hat{\theta}^* + (\hat{\theta}^* - 2\theta_0)^T \mathbf{F}(\hat{\theta}^*) \hat{\theta}^*} + \frac{d\lambda_1(\mathbf{F}(\hat{\theta}^*)) - d}{\lambda_d(\mathbf{F}(\hat{\theta}^*))} \right]\right)$$

where the big  $\mathcal{O}$  notation hides the maximum and minimum eigenvalue of Fisher's information.

Theorem 4 provides insights about the (local) optimality gap, which is tied to the FR norm  $\mathbb{E}[\theta_k^T \mathbf{F}(\hat{\theta}^*) \theta_k]$ , and the gradient variance  $\text{Tr}(\mathbf{C})$ . In other words, the higher the FR norm or the smaller the gradient variance across different training samples, the lower the training loss the model converges to; i.e., the network converges at a faster rate.

### C.1 Proof of Theorem 3

**Lemma 2.** *Assume A.3. The loss function of candidate network  $\ell(\theta; \mathbf{x}, \mathbf{y})$  is locally Lipschitz continuous with a Lipschitz constant  $L$  for any  $(\mathbf{x}, \mathbf{y})$ , that is,  $|\ell(\theta_1; \mathbf{x}, \mathbf{y}) - \ell(\theta_2; \mathbf{x}, \mathbf{y})| \leq L\|\theta_1 - \theta_2\|$  for all  $\theta_1, \theta_2 \in \mathbb{B}$ .*

*Proof.* The differentiability of the loss  $\nabla \ell(\theta; \mathbf{x}, \mathbf{y})$  (Assumption A.3) implies the boundedness of  $\nabla \ell$  on the compact set  $\mathbb{B}$ , i.e.  $\|\nabla \ell(\theta; \mathbf{x}, \mathbf{y})\| \leq L$  for all  $\mathbf{x} \in \mathcal{X}, \mathbf{y} \in \mathcal{Y}$  and  $\theta \in \mathbb{B}$ . Here,  $L$  is a constant that bounds the gradient norm. The result can be obtained directly from the Mean Value Theorem (MVT) that

$$\|\ell(\theta_1, \mathbf{x}, \mathbf{y}) - \ell(\theta_2, \mathbf{x}, \mathbf{y})\| \leq \|\nabla \ell(\xi \theta_1 + (1 - \xi) \theta_2)\| \|\theta_1 - \theta_2\| \leq L_\ell \|\theta_1 - \theta_2\|$$

where  $\xi \in (0, 1)$  is some constant.  $\square$

**Lemma 3** (Theorem 3 Moulines and Bach [2011]). *Under some regularity conditions, for a first-order stochastic gradient descent (4) ( $\mathbf{B}_k = \mathbf{I}$ ), we have:*

$$\mathbb{E}[\|\bar{\theta}_k - \hat{\theta}^*\|^2] \leq \frac{\text{Tr}(\mathbf{H}(\hat{\theta}^*)^{-1} \mathbf{C} \mathbf{H}(\hat{\theta}^*)^{-1})}{k+1} + o\left(\frac{1}{k}\right)$$

where the big  $\mathcal{O}$  notation hides constants such as the upper bound of the norm of the Hessian matrix, strong convexity constant, and Lipschitz constant. We refer to Moulines and Bach [2011] for detailed information about regularity conditions.

**Lemma 4.** (Ruhe's trace inequality Ruhe [1970]). *If  $\mathbf{A}$  and  $\mathbf{B}$  are positive semidefinite Hermitian matrices with eigenvalues,*

$$a_1 \geq a_2 \geq \dots a_d \geq 0 \quad b_1 \geq b_2 \geq \dots b_d \geq 0$$

respectively, then

$$\text{Tr}(\mathbf{A}\mathbf{B}) \leq \sum_{i=1}^d a_i b_i$$

**Lemma 5.** *Let  $\mathbf{A}$  and  $\mathbf{B}$  be two positive semipositive Hermitian matrix with proper dimension for multiplication. We have  $\text{Tr}(\mathbf{A}\mathbf{B}) \leq \text{Tr}(\mathbf{A}) \text{Tr}(\mathbf{B})$ .*

*Proof.* Notice that positive semidefinite implies that all eigenvalues of matrix  $\mathbf{A}$  and  $\mathbf{B}$  are positive. Following Lemma 4, we have

$$\text{Tr}(\mathbf{A}\mathbf{B}) \leq \sum_{i=1}^d a_i b_i \stackrel{(*)}{\leq} \sum_{i=1}^d a_i \sum_{i=1}^d b_i = \text{Tr}(\mathbf{A}) \text{Tr}(\mathbf{B})$$

where  $(*)$  holds due to the fact that  $\sum_{i=1}^d a_i \sum_{i=1}^d b_i = \sum_{i=1}^d a_i b_i + \sum_{i \neq j} a_i b_j \geq \sum_{i=1}^d a_i b_i$  for  $a_i, b_i \geq 0$ .  $\square$

Theorem 3 immediately follows Lemma 3.

**Theorem 3.** *Assume A.1-A.4. If the loss function is strongly convex, under the regularity conditions in Moulines and Bach [2011], for the average iterate  $\bar{\theta}_k = \frac{1}{k+1} \sum_{i=0}^k \theta_i$  with a first-order SGD (4) ( $\mathbf{B}_k = \mathbf{I}$ ), it holds*

$$\mathbb{E}[\ell(\bar{\theta}_k; \mathbf{x}, \mathbf{y}) - \ell(\hat{\theta}^*; \mathbf{x}, \mathbf{y})] \leq L\mathbb{E} \left[ \|\bar{\theta}_k - \hat{\theta}^*\|^2 \right]^{1/2} \leq \mathcal{O} \left( \frac{\text{Tr}(\mathbf{F}(\hat{\theta}^*)^{-1}) \sqrt{\text{Tr}(\mathbf{C})}}{\sqrt{k}} \right) + o \left( \frac{1}{\sqrt{k}} \right)$$

*Proof.* The Lipschitz continuity of the loss function (Lemma 2) with a Lipschitz constant  $L < \infty$  implies that

$$\mathbb{E} \left[ \ell(\bar{\theta}_k) - \ell(\hat{\theta}^*) \right] \leq L\mathbb{E} \left[ \|\bar{\theta}_k - \hat{\theta}^*\| \right] \leq L\mathbb{E} \left[ \|\bar{\theta}_k - \hat{\theta}^*\|^2 \right]^{1/2}$$

Since  $\mathbf{H}$  and  $\mathbf{C}$  are both positive definite, applying Lemma 5 twice leads to

$$\text{Tr} \left( \mathbf{H}(\hat{\theta}^*)^{-1} \mathbf{C} \mathbf{H}(\hat{\theta}^*)^{-1} \right) \leq \text{Tr} \left( \mathbf{H}(\hat{\theta}^*)^{-1} \right)^2 \text{Tr}(\mathbf{C}). \quad (12)$$

Using Lemma 3 and Eq. 12, we have

$$\mathbb{E} \left[ \ell(\bar{\theta}_k) - \ell(\hat{\theta}^*) \right]^2 \leq \frac{L^2 \text{Tr} \left( \mathbf{H}(\hat{\theta}^*)^{-1} \mathbf{C} \mathbf{H}(\hat{\theta}^*)^{-1} \right)}{k+1} + o \left( \frac{1}{k} \right) \leq \frac{L^2 \text{Tr} \left( \mathbf{H}(\hat{\theta}^*)^{-1} \right)^2 \text{Tr}(\mathbf{C})}{k+1} + o \left( \frac{1}{k} \right)$$

Then the conclusion follows the inequality  $\sqrt{a+b} \leq \sqrt{a} + \sqrt{b}$  for  $a, b \geq 0$  and the ‘‘realizability’’ assumption A.1.  $\square$

## C.2 Proof of Theorem 4

To begin with, we present several technical lemmas to support the proof of Theorem 4.

**Lemma 6** (Theorem 1 Bai and Golub [1996]). *Let  $\mathbf{A}$  be an  $d$ -by- $d$  symmetric positive definite matrix,  $\mu_1 = \text{Tr}(\mathbf{A})$ ,  $\mu_2 = \|\mathbf{A}\|_F^2$  and  $\alpha \leq \lambda_d(\mathbf{A}) \leq \dots \leq \lambda_1(\mathbf{A}) \leq \beta$  with  $\alpha > 0$ , then*

$$(\mu_1 \quad d) \begin{pmatrix} \mu_2 & \mu_1 \\ \beta^2 & \beta \end{pmatrix}^{-1} (d \quad 1) \leq \text{Tr}(\mathbf{A}^{-1}) \leq (\mu_1 \quad d) \begin{pmatrix} \mu_2 & \mu_1 \\ \alpha^2 & \alpha \end{pmatrix}^{-1} (d \quad 1) \quad (13)$$

**Lemma 7.** *Suppose that  $\alpha \leq \lambda_1(\mathbf{F}) \leq \beta$ . Then for a  $d$ -by- $d$  symmetric positive definite matrix  $\mathbf{F}$ , it holds that*

$$\text{Tr}(\mathbf{F}^{-1}) \leq d^2 \text{Tr}(\mathbf{F})^{-1} + \frac{d\beta}{\alpha} - \frac{d}{\alpha} \quad (14)$$

*Proof.* Applying Lemma 6 to  $\text{Tr}(\mathbf{F}^{-1})$  leads to

$$\text{Tr}(\mathbf{F}^{-1}) \leq (\text{Tr}(\mathbf{F}) \quad d) \begin{pmatrix} \|\mathbf{F}\|_F^2 & \text{Tr}(\mathbf{F}) \\ \alpha^2 & \alpha \end{pmatrix}^{-1} (d \quad 1) = \frac{d\alpha \cdot \text{Tr}(\mathbf{F}) - d^2\alpha^2 - \text{Tr}(\mathbf{F})^2 + d\|\mathbf{F}\|_F^2}{\alpha\|\mathbf{F}\|_F^2 - \alpha^2 \text{Tr}(\mathbf{F})} \quad (15)$$

where the last equality holds due to the definition of matrix inverse. The Eq. (15) can be further rearranged to

$$\text{Tr}(\mathbf{F}^{-1}) \leq -\frac{d}{\alpha} + \frac{d^2\alpha^2 + \text{Tr}(\mathbf{F})^2}{\alpha^2 \text{Tr}(\mathbf{F}) - \alpha\|\mathbf{F}\|_F^2} \leq -\frac{d}{\alpha} + \frac{d^2\alpha^2 + \text{Tr}(\mathbf{F})^2}{\alpha^2 \text{Tr}(\mathbf{F})} \leq -\frac{d}{\alpha} + \frac{d^2}{\text{Tr}(\mathbf{F})} + \frac{\text{Tr}(\mathbf{F})}{\alpha} \quad (16)$$

The conclusion (14) can be obtained by noting that  $\text{Tr}(\mathbf{F}) = \sum_{i=1}^d \lambda_i(\mathbf{F}) \leq d\beta$ .  $\square$

**Theorem 4** *Assume A.1-A.4. Consider the first order SGD update 4 ( $\mathbf{B}_k = \mathbf{I}$ ) with fixed learning rate  $\eta$ . If the loss function is strongly convex, under the same assumption as stated in Lemma 3, the expected loss is bounded as follows*

$$\begin{aligned} & \mathbb{E}[\ell(\bar{\theta}_k; \mathbf{x}, \mathbf{y})] - \mathbb{E}[\ell(\hat{\theta}^*; \mathbf{x}, \mathbf{y})] \\ & \leq \mathcal{O} \left( \frac{\sqrt{\text{Tr}(\mathbf{C})}}{2\sqrt{k+1}} \left[ \frac{d^2 M}{\mathbb{E}[\theta_k \mathbf{F}(\hat{\theta}^*) \theta_k] + 2\eta \mathbb{E}[\sum_{i=0}^k \nabla \ell(\theta_i; \mathcal{D}_i)]^\top \mathbf{F}(\hat{\theta}^*) \hat{\theta}^* + (\hat{\theta}^* - 2\theta_0)^\top \mathbf{F}(\hat{\theta}^*) \hat{\theta}^*} + \frac{d\lambda_1(\mathbf{F}(\hat{\theta}^*)) - d}{\lambda_d(\mathbf{F}(\hat{\theta}^*))} \right] \right) \end{aligned}$$

where the big  $\mathcal{O}$  notation hides the maximum and minimum eigenvalue of Fisher’s information.

*Proof.* To begin with, we have

$$\mathrm{Tr} \left( \mathbf{F}(\hat{\boldsymbol{\theta}}^*)^{-1} \right) \leq \frac{d^2}{\mathrm{Tr}(\mathbf{F}(\hat{\boldsymbol{\theta}}^*))} + \frac{d\lambda_1(\mathbf{F}(\hat{\boldsymbol{\theta}}^*)) - d}{\lambda_d(\mathbf{F}(\hat{\boldsymbol{\theta}}^*))} \quad (17)$$

where the inequality holds because of Lemma 7 and choosing  $\alpha = \lambda_d(\mathbf{F})$  and  $\beta = \lambda_1(\mathbf{F})$ . Further, note that

$$\begin{aligned} \mathbb{E} \left[ \mathrm{Tr} \left( (\boldsymbol{\theta}_k - \hat{\boldsymbol{\theta}}^*)^\top \mathbf{F}(\hat{\boldsymbol{\theta}}^*) (\boldsymbol{\theta}_k - \hat{\boldsymbol{\theta}}^*) \right) \right] &= \mathbb{E} \left[ \mathrm{Tr} \left( \mathbf{F}(\hat{\boldsymbol{\theta}}^*) (\boldsymbol{\theta}_k - \hat{\boldsymbol{\theta}}^*) (\boldsymbol{\theta}_k - \hat{\boldsymbol{\theta}}^*)^\top \right) \right] \\ &\leq \mathrm{Tr} \left( \mathbf{F}(\hat{\boldsymbol{\theta}}^*) \right) \mathbb{E} \left[ \mathrm{Tr} \left( (\boldsymbol{\theta}_k - \hat{\boldsymbol{\theta}}^*) (\boldsymbol{\theta}_k - \hat{\boldsymbol{\theta}}^*)^\top \right) \right] \end{aligned} \quad (18)$$

Notice that  $\mathrm{Tr} \left( (\boldsymbol{\theta}_k - \hat{\boldsymbol{\theta}}^*) (\boldsymbol{\theta}_k - \hat{\boldsymbol{\theta}}^*)^\top \right) = \|\boldsymbol{\theta}_k - \hat{\boldsymbol{\theta}}^*\|^2$ . Then Eq. 18 becomes

$$\begin{aligned} \frac{1}{\mathrm{Tr} \left( \mathbf{F}(\hat{\boldsymbol{\theta}}^*) \right)} &\leq \frac{\mathbb{E} \left[ \|\boldsymbol{\theta}_k - \hat{\boldsymbol{\theta}}^*\|^2 \right]}{\mathbb{E} \left[ \mathrm{Tr} \left( (\boldsymbol{\theta}_k - \hat{\boldsymbol{\theta}}^*)^\top \mathbf{F}(\hat{\boldsymbol{\theta}}^*) (\boldsymbol{\theta}_k - \hat{\boldsymbol{\theta}}^*) \right) \right]} \\ &= \frac{\mathbb{E} \left[ \|\boldsymbol{\theta}_k - \hat{\boldsymbol{\theta}}^*\|^2 \right]}{\mathbb{E} \left[ \boldsymbol{\theta}_k^\top \mathbf{F}(\hat{\boldsymbol{\theta}}^*) \boldsymbol{\theta}_k \right] - 2\mathbb{E} \left[ \boldsymbol{\theta}_k^\top \mathbf{F}(\hat{\boldsymbol{\theta}}^*) \hat{\boldsymbol{\theta}}^* \right] + \hat{\boldsymbol{\theta}}^{*\top} \mathbf{F}(\hat{\boldsymbol{\theta}}^*) \hat{\boldsymbol{\theta}}^*} \end{aligned} \quad (19)$$

Notice that  $\boldsymbol{\theta}_k = \boldsymbol{\theta}_0 - \eta \sum_{i=0}^k \mathbf{g}(\boldsymbol{\theta}_i)$  and thus

$$-\mathbb{E} \left[ \boldsymbol{\theta}_k^\top \mathbf{F}(\hat{\boldsymbol{\theta}}^*) \hat{\boldsymbol{\theta}}^* \right] = -\boldsymbol{\theta}_0^\top \mathbf{F}(\hat{\boldsymbol{\theta}}^*) \hat{\boldsymbol{\theta}}^* + \eta \mathbb{E} \left[ \left[ \sum_{i=0}^k \mathbf{g}(\boldsymbol{\theta}_i) \right]^\top \mathbf{F}(\hat{\boldsymbol{\theta}}^*) \hat{\boldsymbol{\theta}}^* \right] \quad (20)$$

Then combining Eq. 19 and Eq. 20, we have

$$\frac{1}{\mathrm{Tr} \left( \mathbf{F}(\hat{\boldsymbol{\theta}}^*) \right)} \leq \frac{M}{\mathbb{E} \left[ \boldsymbol{\theta}_k^\top \mathbf{F}(\hat{\boldsymbol{\theta}}^*) \boldsymbol{\theta}_k \right] + 2\eta \mathbb{E} \left[ \sum_{i=0}^k \mathbf{g}(\boldsymbol{\theta}_i) \right]^\top \mathbf{F}(\hat{\boldsymbol{\theta}}^*) \hat{\boldsymbol{\theta}}^* + (\boldsymbol{\theta}^* - 2\boldsymbol{\theta}_0)^\top \mathbf{F}(\hat{\boldsymbol{\theta}}^*) \hat{\boldsymbol{\theta}}^*}$$

By applying the equation above to Eq. 17, we further have

$$\begin{aligned} \mathrm{Tr}(\mathbf{F}^{-1}(\hat{\boldsymbol{\theta}}^*)) &\leq \frac{d^2 M}{\mathbb{E} \left[ \boldsymbol{\theta}_k^\top \mathbf{F}(\hat{\boldsymbol{\theta}}^*) \boldsymbol{\theta}_k \right] + 2\eta \mathbb{E} \left[ \sum_{i=0}^k \mathbf{g}(\boldsymbol{\theta}_i) \right]^\top \mathbf{F}(\hat{\boldsymbol{\theta}}^*) \hat{\boldsymbol{\theta}}^* + (\boldsymbol{\theta}^* - 2\boldsymbol{\theta}_0)^\top \mathbf{F}(\hat{\boldsymbol{\theta}}^*) \hat{\boldsymbol{\theta}}^*} \\ &\quad + \frac{d\lambda_1(\mathbf{F}(\hat{\boldsymbol{\theta}}^*)) - d}{\lambda_d(\mathbf{F}(\hat{\boldsymbol{\theta}}^*))} \end{aligned}$$

The conclusion can be immediately obtained by applying Theorem 3.  $\square$

## D Proof of Theorem 2

**Theorem 2** Assume A.1-A.4. Let  $\mu_k = \sum_{i=0}^k \mathbb{E} [\|\nabla \ell(\boldsymbol{\theta}_i; \mathcal{D}_i)\|_1]$  denote the sum of the expected absolute value of gradient across mini-batch samples, denoted by  $\mathcal{D}_i$ , where the gradient norm is

$$\|\nabla \ell(\boldsymbol{\theta}_i; \mathcal{D}_i)\|_1 = \sum_{j=1}^d \left| \nabla_{\theta_i^{(j)}} \ell(\boldsymbol{\theta}_i; \mathcal{D}_i) \right| \quad \text{and} \quad \nabla_{\theta_i^{(j)}} \ell(\boldsymbol{\theta}_i; \mathcal{D}_i) = \frac{1}{|\mathcal{D}_i|} \sum_{n=1}^{|\mathcal{D}_i|} \nabla_{\theta_i^{(j)}} \ell(\boldsymbol{\theta}_i; \mathbf{x}_n, \mathbf{y}_n).$$

Under some regularity conditions such that  $\mathbb{E} \left[ (\boldsymbol{\theta}_k - \hat{\boldsymbol{\theta}}^*)^3 \right] = o\left(\frac{1}{k}\right)$ , it holds

$$\mathcal{L}(\hat{\boldsymbol{\theta}}^*) \geq \mathbb{E}[\mathcal{L}(\boldsymbol{\theta}_k)] - \frac{1}{2} \mathbb{E} \left[ \boldsymbol{\theta}_k^\top \mathbf{F}(\hat{\boldsymbol{\theta}}^*) \boldsymbol{\theta}_k \right] - \eta \mu_k \|\mathbf{H}(\hat{\boldsymbol{\theta}}^*) \hat{\boldsymbol{\theta}}^*\|_\infty - \frac{1}{2} (\hat{\boldsymbol{\theta}}^* - 2\boldsymbol{\theta}_0)^\top \mathbf{H}(\hat{\boldsymbol{\theta}}^*) \hat{\boldsymbol{\theta}}^* + o\left(\frac{1}{k}\right).$$

*Proof.* Notice that the optimality gap is  $G(\boldsymbol{\theta}_k) := \mathbb{E}[\mathcal{L}(\boldsymbol{\theta}_k)] - \mathcal{L}(\hat{\boldsymbol{\theta}}^*)$ . By applying Taylor approximation up to second order in Eq. 6 and taking expectation over the filtration, we have

$$\begin{aligned} G(\boldsymbol{\theta}_k) &= \frac{1}{2} \mathbb{E} \left[ \boldsymbol{\theta}_k^\top \mathbf{H}(\hat{\boldsymbol{\theta}}^*) \boldsymbol{\theta}_k - 2\boldsymbol{\theta}_k^\top \mathbf{H}(\hat{\boldsymbol{\theta}}^*) \hat{\boldsymbol{\theta}}^* + \boldsymbol{\theta}^{*\top} \mathbf{H}(\hat{\boldsymbol{\theta}}^*) \hat{\boldsymbol{\theta}}^* \right] + \mathbb{E} \left[ \mathcal{O} \left( (\boldsymbol{\theta}_k - \hat{\boldsymbol{\theta}}^*)^3 \right) \right] \\ &= \frac{1}{2} \mathbb{E} \left[ \boldsymbol{\theta}_k^\top \mathbf{H}(\hat{\boldsymbol{\theta}}^*) \boldsymbol{\theta}_k \right] + \eta \mathbb{E} \left[ \sum_{i=0}^k \mathbf{g}(\boldsymbol{\theta}_i) \right]^\top \mathbf{H}(\hat{\boldsymbol{\theta}}^*) \hat{\boldsymbol{\theta}}^* + \frac{1}{2} (\boldsymbol{\theta}^* - 2\boldsymbol{\theta}_0)^\top \mathbf{H}(\hat{\boldsymbol{\theta}}^*) \hat{\boldsymbol{\theta}}^* + o \left( \frac{1}{k} \right). \end{aligned}$$

Then by replacing Hessian with Fisher information matrix in the first term, the optimality gap is bounded as follows

$$G(\boldsymbol{\theta}_k) \leq \frac{E \left[ \boldsymbol{\theta}_k^\top \mathbf{F}(\hat{\boldsymbol{\theta}}^*) \boldsymbol{\theta}_k \right]}{2} + \eta \mathbb{E} \left[ \sum_{i=0}^k \mathbf{g}(\boldsymbol{\theta}_i) \right]^\top \mathbf{H}(\hat{\boldsymbol{\theta}}^*) \hat{\boldsymbol{\theta}}^* + \frac{(\boldsymbol{\theta}^* - 2\boldsymbol{\theta}_0)^\top \mathbf{H}(\hat{\boldsymbol{\theta}}^*) \hat{\boldsymbol{\theta}}^*}{2} + o \left( \frac{1}{k} \right) \quad (21)$$

By applying Hölder’s inequality and Minkowski’s Inequality, the second term in Eq. 21 is

$$\mathbb{E} \left[ \sum_{i=0}^k \mathbf{g}(\boldsymbol{\theta}_i) \right]^\top \mathbf{H}(\hat{\boldsymbol{\theta}}^*) \hat{\boldsymbol{\theta}}^* \leq \mathbb{E} \left[ \left\| \sum_{i=0}^k \mathbf{g}(\boldsymbol{\theta}_i) \right\|_1 \right] \left\| \mathbf{H}(\hat{\boldsymbol{\theta}}^*) \hat{\boldsymbol{\theta}}^* \right\|_\infty \leq \sum_{i=0}^k \mathbb{E} [\|\mathbf{g}(\boldsymbol{\theta}_i)\|_1] \left\| \mathbf{H}(\hat{\boldsymbol{\theta}}^*) \hat{\boldsymbol{\theta}}^* \right\|_\infty.$$

Therefore, since  $\mu_k = \sum_{i=0}^k \mathbb{E} [\|\mathbf{g}(\boldsymbol{\theta}_i)\|_1]$  we have

$$G(\boldsymbol{\theta}_k) \leq \frac{1}{2} \mathbb{E} \left[ \boldsymbol{\theta}_k^\top \mathbf{F}(\hat{\boldsymbol{\theta}}^*) \boldsymbol{\theta}_k \right] + \eta \mu_k \left\| \mathbf{H}(\hat{\boldsymbol{\theta}}^*) \hat{\boldsymbol{\theta}}^* \right\|_\infty + \frac{1}{2} (\boldsymbol{\theta}^* - 2\boldsymbol{\theta}_0)^\top \mathbf{H}(\hat{\boldsymbol{\theta}}^*) \hat{\boldsymbol{\theta}}^* + o \left( \frac{1}{k} \right)$$

from which the conclusion immediately follows.  $\square$

## E Practical Implementation

While SiGeo necessitates a well-executed initialization in contrast to other zero-shot proxies, our experimental results indicate that the training-free SiGeo is capable of achieving comparable or superior performance to the SOTA zero-shot proxies across all computer vision tasks.

**Proxy Weights.** In all instances, we consistently set the value of  $\lambda_1$  to 1. However, the selection of  $\lambda_2$  and  $\lambda_3$  values varies depending on the specific search space and the warm-up level. Specifically, for candidate architectures without warm-up, we adjust our proxy by setting  $\lambda_2 = 1$  and  $\lambda_3 = 0$  to account for significant noise in training loss values and the reduced effectiveness of the Fisher-Rao (FR) norm. Conversely, if a warm-up procedure is performed, we opt for  $\lambda_2 = \lambda_3 = 1$  in RecSys search spaces, while for CV benchmarks, we use  $\lambda_{50} = 50$  and  $\lambda_3 = 1$ . The larger value of  $\lambda_2$  for CV benchmarks is due to the observation that the zico scores of CNN models are significantly larger than those of networks in the NASRec search space.

**FR Norm.** The FR norm can be efficiently computed by the average of squared product of parameters and gradients:  $\boldsymbol{\theta}_k \bar{\mathbf{F}} \boldsymbol{\theta}_k = \frac{1}{k} \sum_{i=1}^k \boldsymbol{\theta}_k \nabla \ell(\boldsymbol{\theta}; \mathcal{D}_i) \nabla \ell(\boldsymbol{\theta}; \mathcal{D}_i)^\top \boldsymbol{\theta}_k^\top = \frac{1}{k} \sum_{i=1}^k (\boldsymbol{\theta}_k^\top \nabla \ell(\boldsymbol{\theta}; \mathcal{D}_i))^2$

## F Implementation Details

### F.1 Experiment (1): Empirical Justification for Theorem 4 and Theorem 2

We conducted training using a two-layer MLP equipped with ReLU activation functions across the complete MNIST training dataset for three epochs. The weights were updated through the application of gradient descent as per Equation 4, employing a batch size of 128. Throughout training, these networks were optimized using the SGD optimizer with a learning rate of 0.01.

In the preprocessing phase, all image tensors were normalized using a mean of (0.4914, 0.4822, 0.4465) and a standard deviation of (0.2023, 0.1994, 0.2010). Following these preparations, SiGeo scores were computed using four training batches after the candidate architectures were trained on 0, 48, and 192 batches, corresponding to 0%, 10% and 40% warm-up levels. Then we visualize the relationship of the training loss and test loss after three training epochs vs. (i) current training loss, (ii) FR norm and (iii) mean absolute sample gradients in Fig 5-7 in Appendix G

## F.2 Experiment (2) and (3): Comparing SiGeo with Other Proxies on NAS Benchmarks

To calculate the correlations, we utilize the NAS-Bench-Suite-Zero [Krishnakumar et al., 2022]. This suite encompasses a comprehensive set of commonly used zero-shot proxies, complete with their official codebases released by the original authors, enabling us to accurately obtain the proxy values. Since the ZiCo proxy was not incorporated into NAS-Bench-Suite-Zero, we employed its official code to compute the correlations for ZiCo.

In the zero-shot setting, we adjust our proxy by setting  $\lambda_2 = 1$  and  $\lambda_3 = 0$ . If a warm-up procedure is performed, we set we use  $\lambda_{50} = 50$  and  $\lambda_3 = 1$ . The larger value of  $\lambda_2$  for CV benchmarks is due to the observation that the zico scores of CNN models are significantly larger (roughly 50 times greater) than those of networks in the NASRec search space.

## F.3 Experiment (4): RecSys Benchmark Results

During this process, we train the supernet for a single epoch, employing the Adagrad optimizer, an initial learning rate of 0.12, and a cosine learning rate schedule on target RecSys benchmarks. We refer readers to Zhang et al. [2023] for the details about the search space, search policy, and training strategy.

**Regularized Evolution.** Following Zhang et al. [2023], we employ an efficient configuration of regularized evolution to find the optimal subnets from the supernet. Specifically, we keep 128 architectures in a population and run the regularized evolution algorithm for 240 iterations. In each iteration, we select the best design from 64 sampled architectures as the parent architecture, then create 8 new child architectures to update the population.

## F.4 Experiment (5): SiGeo v.s. Other Proxies on CIFAR-10/CIFAR-100

The experimental setup in this section mirrors that of Lin et al. [2021a], and is outlined below:

**Dataset** CIFAR-10 comprises 50,000 training images and 10,000 testing images, divided into 10 classes, each with a resolution of 32x32 pixels. CIFAR-100 follows a similar structure with the same number of training and testing images but contains 100 distinct classes. ImageNet1k, on the other hand, has over 1.2 million training images and 50,000 validation images across 1000 classes. In our experiments, we use the official training/validation split.

**Augmentation** We use the following augmentations as in [Pham et al., 2018]: mix-up [Zhang et al., 2018], label-smoothing [Szegedy et al., 2016], random erasing [Zhong et al., 2020], random crop/resize/flip/lighting and AutoAugment [Cubuk et al., 2019].

**Optimizer** For all experiments in Experiment (3), we use SGD optimizer with momentum 0.9; weight decay  $5e-4$  for CIFAR10/100; initial learning rate 0.1 with batch size 256; cosine learning rate decay [Loshchilov and Hutter, 2017]. We train models up to 1440 epochs in CIFAR-10/100. Following previous works [Aguilar et al., 2020, Li et al., 2020], we use EfficientNet-B3 as teacher networks.

In each run, the starting structure is a randomly chosen small network that adheres to the imposed inference budget. The search for kernel sizes is conducted within the set  $\{3, 5, 7\}$ . Consistent with traditional design practices, there are three stages for CIFAR-10/CIFAR-100/ The evolutionary process involves a population size of 512 and a total of 480,000 evolutionary iterations. For CIFAR-10/CIFAR-100, the resolution is 32x32.

**Model Selection** During weight-sharing neural architecture evaluation, we train the supernet on the training set and select the top 15 subnets on the validation set. Then we train the top-15 models from scratch and select the best subnet as the final architecture.

## G Additional Empirical Results for Theorem 4 and Theorem 2

Here we conduct additional assessments in the other two distinct settings: one without any warm-up (Fig. 5) and another with various warm-up levels (Fig. 7). In the absence of warm-up, all four statistics are computed based on the initial four batches. In the case of warm-up, these statistics are calculated using four batches following the initial 196 batches.

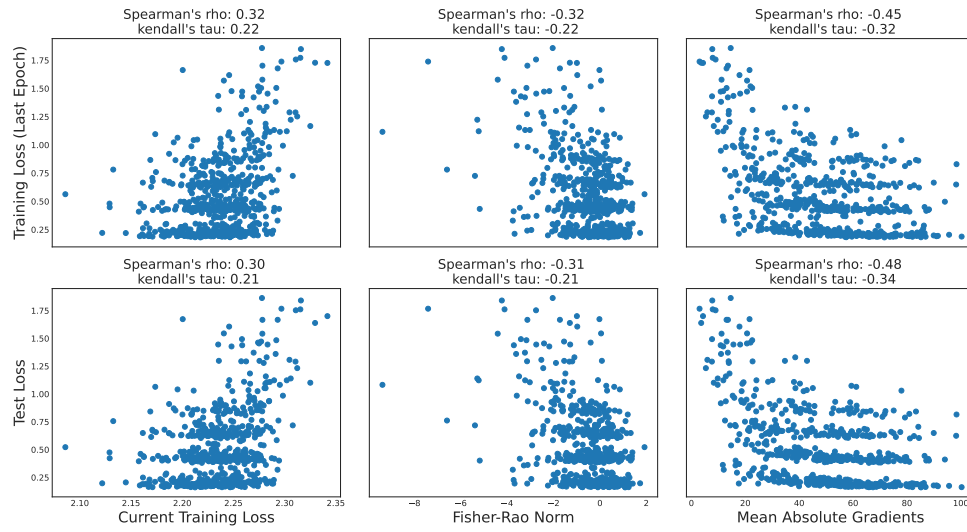


Figure 5: Training and test losses vs. different statistics in Theorem 4 and 2. Results are generated by optimizing two-layer MLP-ReLU networks with varying hidden dimensions, ranging from 2 to 48 in increments of 2. The statistics for each network are computed without warm-up.

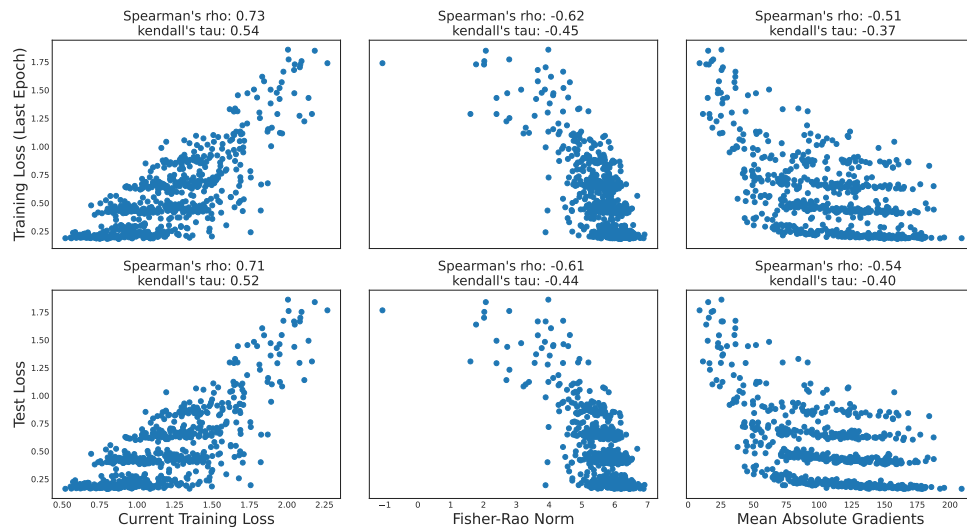


Figure 6: Training/test losses vs. statistics in Theorem 4 and 2. Results are generated by optimizing two-layer MLP-ReLU networks with varying hidden dimensions, ranging from 2 to 48 in increments of 2. The statistics for each network are computed after being warmed up with 10% training data.

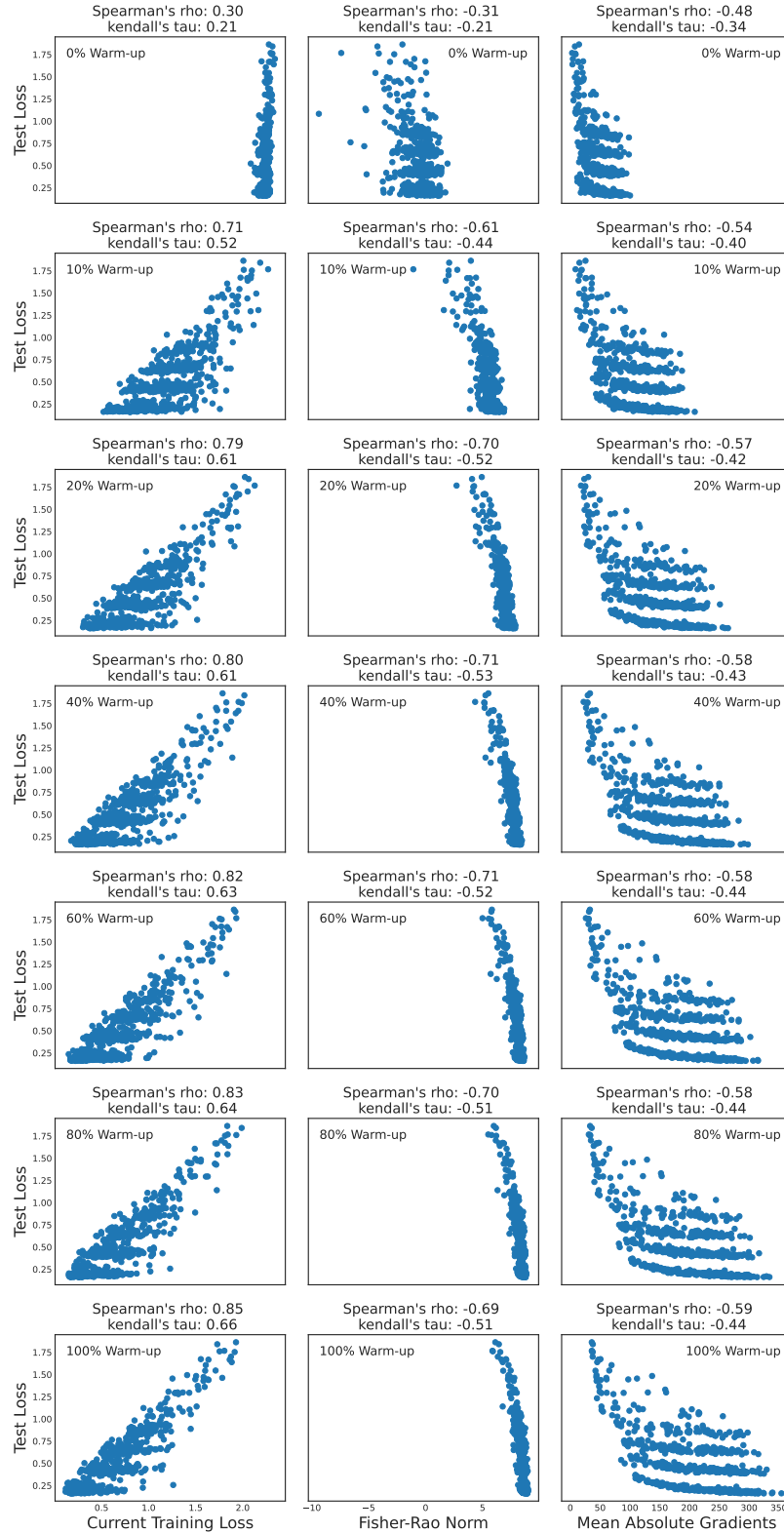


Figure 7: Test losses vs. statistics in Theorem 2. Results are generated by optimizing two-layer MLP-ReLU networks with varying hidden dimensions, ranging from 2 to 48 in increments of 2. The statistics for each network are computed after being warmed up with 0%, 10%, 40%, 60%, 80%, and 100% data. The performance improvement in the FR norm is observed to cease after 40% warm-up.

## H SiGeo v.s. Other Proxies on CIFAR-10/CIFAR-100

Experiments on CIFAR-10/CIFAR-100 [Krizhevsky et al., 2009] are conducted to validate the effectiveness of SiGeo on zero-shot setting. This experiment serves as a compatibility test for SiGeo on zero-shot NAS. To maintain consistency with prior studies, we adopt the search space and training settings outlined in Lin et al. [2021a] to validate SiGeo across both CIFAR-10 and CIFAR-100 datasets. The selected search space, introduced in [He et al., 2016, Radosavovic et al., 2020], comprises residual blocks and bottleneck blocks that are characteristic of the ResNet architecture. We limit the network parameters to 1.0 million. Results are obtained in the *zero-shot setting*: in each trial, the subnet structure is selected from a randomly initialized supernet (without warm-up) under the inference budget; see details in Appendix F.4. Then we use a batch size of 64 and employ four batches to compute both SiGeo and ZiCo. In Table 4, we contrast various NAS-designed models for CIFAR-10/CIFAR-100, and notably, SiGeo outperforms all the baseline methods.

Table 4: Top-1 accuracies on CIFAR-10/CIFAR-100 for zero-shot proxies with a 1M parameter budget. The accuracies for both SiGeo and ZiCo are computed by averaging results from three separate runs. Other scores are adapted from Lin et al. [2021a].

Proxy	Random	FLOPs	grad-norm	synflow	NASWOT	Zen	Zico	SiGeo
CIFAR-10	93.50%	93.10%	92.80%	96.10%	96.00%	96.2%	96.96%	97.01%
CIFAR-100	71.10%	64.70%	65.40%	75.90%	77.50%	80.10%	81.12%	81.19%

## I Additional Result for RecSys Benchmarks

We train NASRecNet from scratch on three classic RecSys benchmarks and compare the performance of models that are crafted by NASRec on three general RecSys benchmarks. In Table 5, we report the evaluation results of our end-to-end NASRecNets and a random search baseline which randomly samples and trains models in our NASRec search space.

Table 5: Performance of SiGeo-NAS on CTR Predictions Tasks. NASRec-Small and NASRec-Full are the two search spaces, and NASRecNet is the NAS method from Zhang et al. [2023].

Setting	Method	Criteo		Avazu		KDD Cup 2012		Search Cost (GPU days)
		Log Loss	AUC	Log Loss	AUC	Log Loss	AUC	
Hand-crafted Arts	DLRM [Naumov et al., 2019]	0.4436	0.8085	0.3814	0.7766	0.1523	0.8004	-
	xDeepFM [Lian et al., 2018]	0.4418	0.8052	-	-	-	-	-
	AutoInt+ [Song et al., 2019]	0.4427	0.8090	0.3813	0.7772	0.1523	0.8002	-
	DeepFM [Guo et al., 2017]	0.4432	0.8086	0.3816	0.7757	0.1529	0.7974	-
NAS-crafted Arts (one-shot) (100% warm-up)	DNAS [Krishna et al., 2021]	0.4442	-	-	-	-	-	~0.28
	PROFIT [Gao et al., 2021]	0.4427	0.8095	<b>0.3735</b>	<b>0.7883</b>	-	-	~0.5
	AutoCTR [Song et al., 2020]	0.4413	0.8104	0.3800	0.7791	0.1520	0.8011	~0.75
	Random Search @ NASRec-Small	0.4411	0.8105	0.3748	0.7885	0.1500	0.8123	1.0
	Random Search @ NASRec-Full	0.4418	0.8098	0.3767	0.7853	0.1509	0.8071	1.0
	NASRecNet @ NASRec-Small	<b>0.4395</b>	<b>0.8119</b>	0.3741	0.7897	0.1489	0.8161	~0.25
	NASRecNet @ NASRec-Full	0.4404	0.8109	0.3736	0.7905	0.1487	0.8170	~0.3
SiGeo @ NASRec-Small	0.4399	0.8115	0.3743	0.7894	0.1487	0.8171	~0.1	
SiGeo @ NASRec-Full	0.4403	0.8110	0.3741	0.7898	0.1484	0.8187	~0.12	
NAS-crafted Arts (sub-one-shot) (1% warm-up)	ZiCo @ NASRec-Small	0.4404	0.8109	0.3754	0.7876	0.1490	0.8164	~0.1
	ZiCo @ NASRec-Full	0.4403	0.8100	0.3762	0.7860	0.1486	0.8174	~0.12
	SiGeo @ NASRec-Small	0.4396	0.8117	<b>0.3741</b>	<b>0.7898</b>	<b>0.1484</b>	<b>0.8185</b>	~0.1
	SiGeo @ NASRec-Full	<b>0.4397</b>	<b>0.8116</b>	0.3754	0.7876	<b>0.1485</b>	<b>0.8178</b>	~0.12
NAS-crafted Arts (zero-shot) (0% warm-up)	ZiCo @ NASRec-Small	0.4408	0.8105	0.3770	0.7849	0.1491	0.8156	~0.09
	ZiCo @ NASRec-Full	0.4404	0.8108	0.3772	0.7845	0.1486	0.8177	~0.11
	SiGeo @ NASRec-Small	0.4404	0.8109	0.3750	0.7882	0.1489	0.8165	~0.09
	SiGeo @ NASRec-Full	0.4404	0.8108	0.3765	0.7856	0.1486	0.8177	~0.11